AD-A054 986 IIT RESEARCH INST CHICAGO ILL F/G 6/18
ELF ELECTRIC FIELD ANALYSIS FOR A LABORATORY BIOLOGICAL EXPERIM--ETC(U)
MAY 78 Y SHIAU N00039-76-C-0141
UNCLASSIFIED IITRI-E6357-9 NL

1 OF 1
AD A054986

END
DATE FILMED
7-78
DDC

Technical Report E6357-9
Contract N00039-76-C-0141

IITRI

ELF ELECTRIC FIELD ANALYSIS FOR A LABORATORY BIOLOGICAL EXPERIMENT.

Y. Shiau

May 1978

70 P.

Prepared for:

U.S. Naval Electronic Systems Command
Washington, D.C.

Submitted by:

IIT Research Institute
10 West 35th Street
Chicago, Illinois 60616

FOREWORD

This document was prepared for the Special Communications Project Office of the U.S. Naval Electronic Systems Command by IIT Research Institute under Contract N00039-76-C-0141.

The technical effort reported herein is intended to support biological studies in connection with the Navy's Seafarer ELF communications system. The report covers an analysis of the electric field levels induced in individual tissue culture samples when exposed to uniform electric and magnetic fields in a laboratory simulator. Calculations are included to derive sample field levels for the NMRI tissue culture experiment. A companion report "ELF Electric and Magnetic Field Simulation for a Laboratory Biological Experiment," IITRI Technical Report E6357-10, describes the field simulator developed by IITRI for the NMRI experiment.

Respectfully submitted,

IIT RESEARCH INSTITUTE

Y. Shiau
Associate Engineer

APPROVED:

R. D. Carlson
Program Manager

A. R. Valentino
Manager, EM Effects

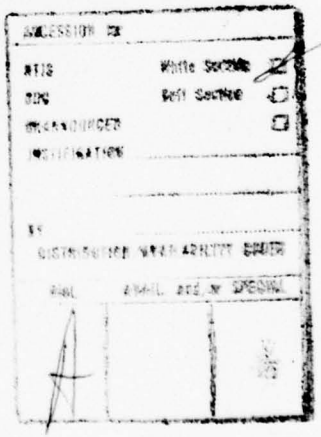

TABLE OF CONTENTS

*Due to the considerable commonality between the main text and the four appendices, all references are given at the end of the report.

LIST OF TABLES AND FIGURES

LIST OF TABLES AND FIGURES (Cont.)

1. INTRODUCTION

Modern technology has developed many applications for radio frequency and microwave electromagnetic energy. These applications include communications, remote detection, industrial processing, food preparation, and medical diagnosis and therapy. This extensive usage has led to concern about the potential for biological hazards from electromagnetic radiation exposure and to the setting of national standards for the maximum permissible exposure for humans.[1] The possible effects on organisms of extremely low frequency (ELF, 20 to 100 Hz) electric and magnetic fields are also being studied. This research includes the Navy's proposed ELF Communications System[2,3] as well as power systems.[4] The research spans a broad spectrum of biological sciences, from enzymes to mammalian behavior, and from bacteria and slime molds to primates.

Recently, research has been initiated at the Naval Medical Research Institute (NMRI) to study the possible effects of the electric and magnetic fields associated with the Navy's proposed ELF Communications System (Seafarer) on human tissue cultures. The necessary electrical engineering support for this experiment is provided by the IIT Research Institute (IITRI). The apparatus used to generate and control the required electric and magnetic fields was designed, fabricated and installed by IITRI. In support of this design, an analysis was performed to determine the field internal to the tissue culture as a function of applied field and exposure geometry. The purpose of this report is to present the details of this analysis. A companion report[5] discusses the design and operation of the electric and magnetic field simulator.

The ELF electromagnetic field simulator designed for tissue experiments at NMRI employs parallel plates to generate a uniform electric field and a multi-coil to provide a uniform magnetic field. A photograph of this simulator is shown in Figure 1. The tissue under test is normally placed in a plastic tissue culture tray. The photograph of Figure 2 illustrates one of these tissue culture trays.

In the test volume of the simulator, both electric and magnetic fields are induced inside the biological tissue. The important aspect of the present problem of electromagnetic coupling and interaction is

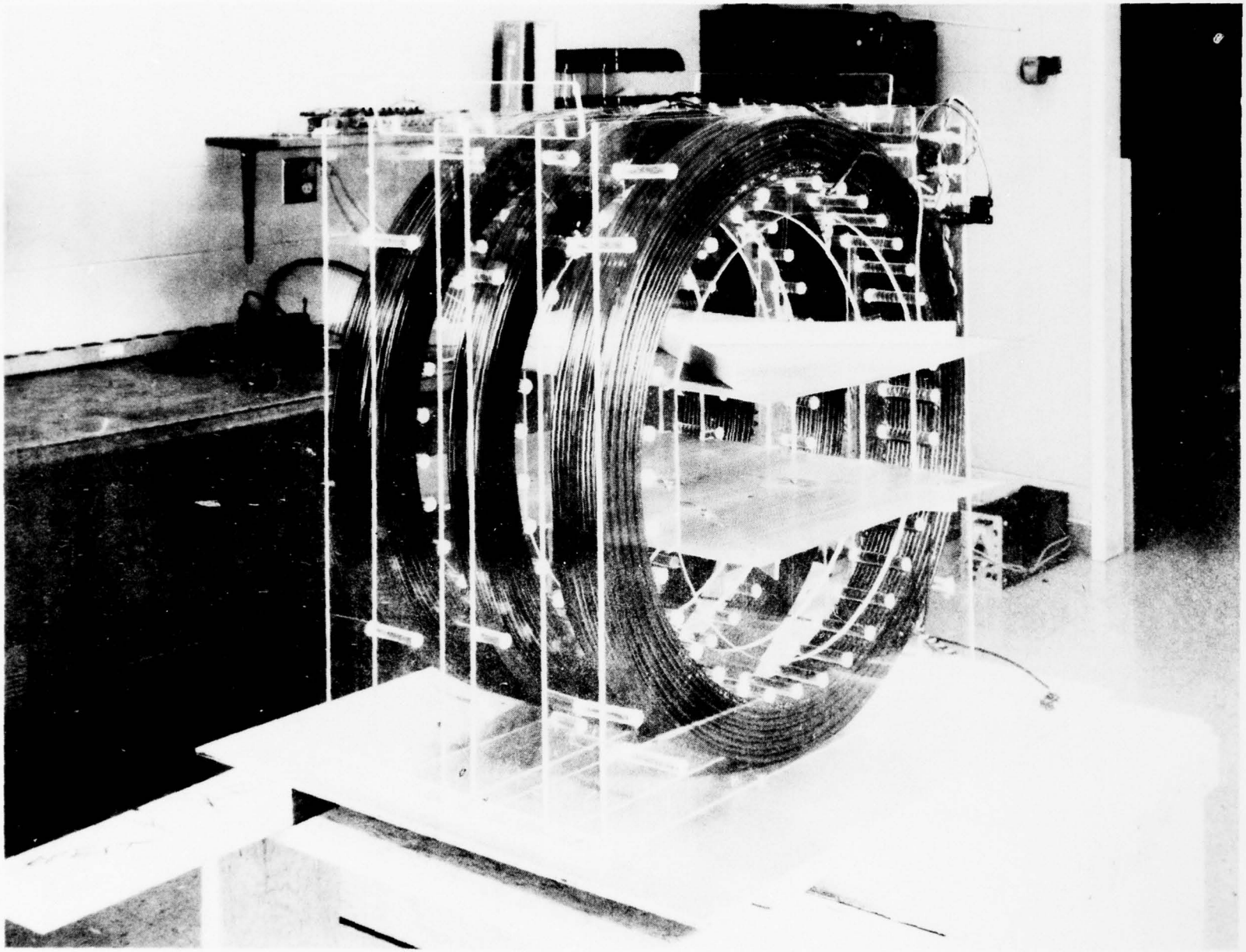

Fig 1 THE ELF ELECTROMAGNETIC FIELD SIMULATOR
DESIGNED FOR THE TISSUE EXPERIMENTS AT NMRI

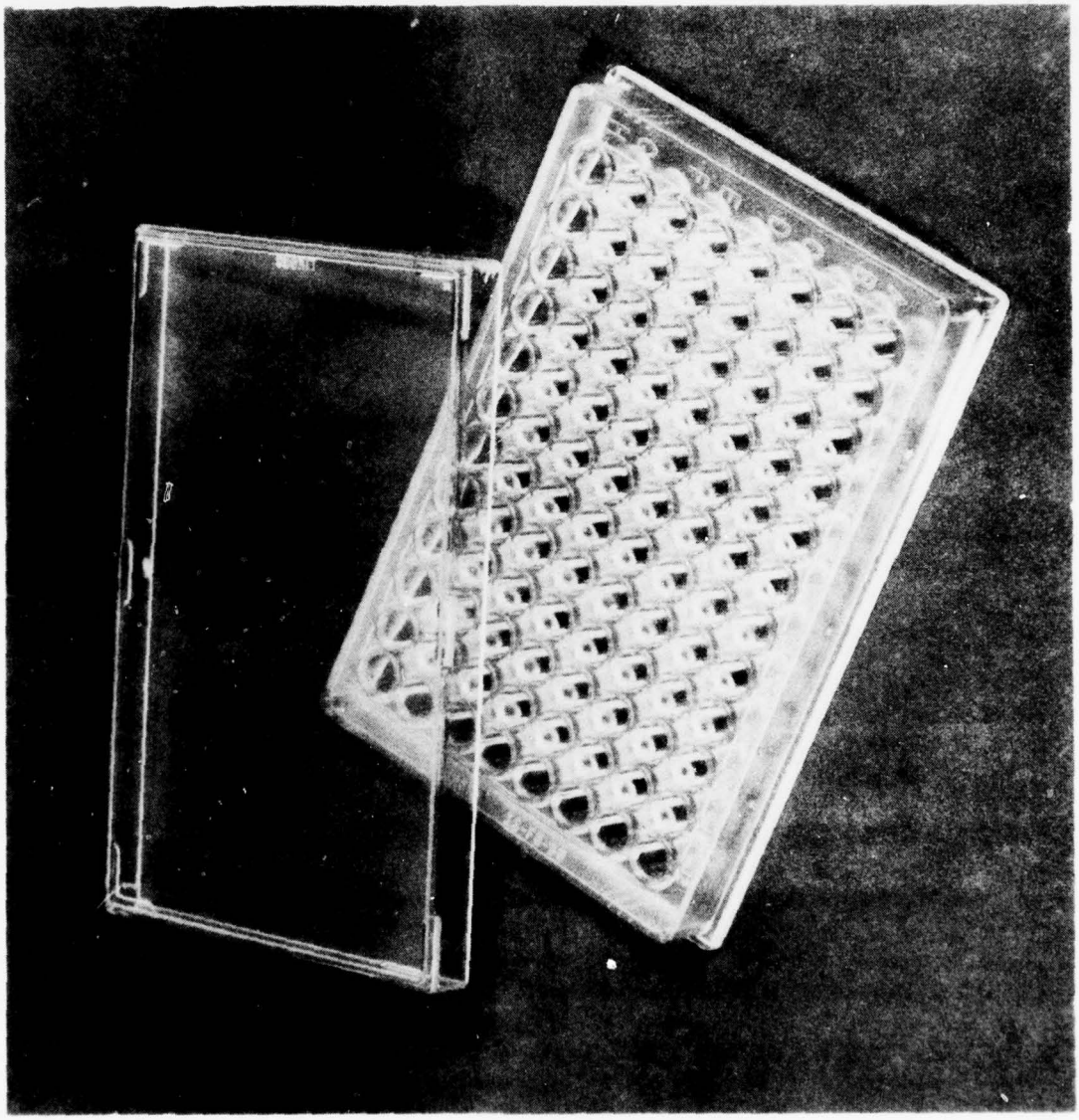

Fig. 2 A TISSUE CULTURE TRAY FOR THE EXPERIMENTS AT NMRI

the determination of the electric field strength and the magnetic field strength induced inside the tissue culture. For the case of present interest, the magnetic field inside the tissue culture has a magnitude equal to that of the impressed field, and suffers no significant distortion because the frequency of interest is low and the permeabilities of the biological tissue and their surrounding medium are essentially that of free space. To determine the electric field strength internal to the biological tissue, we must either conduct an experimental measurement or develop a theoretical analysis. For the periodic lattice structure (see Figure 2) considered here, it is difficult to accurately measure the internal electric field strength because of the fact that the electric field strength internal to a very high permittivity object is low, and because the test specimens are small. As a result, the electric field coupled into the biological tissue in the plastic tray of Figure 2 must be determined analytically.

The purpose of this study then is to analytically determine the electric field induced inside biological objects which are embedded inside a dielectric slab in a periodic fashion. Specifically, we want to know quantitatively the electric field strength inside the tissue culture when the tissue culture tray is exposed to the uniform electric field generated by the simulator.

The biological object, characterized by the constitutive parameters ε_1, μ_1, is assumed to be homogeneous and isotropic where ε_1 is the permittivity and μ_1 is the permeability of the biological tissue. The surrounding dielectric medium in which the objects are embedded is also homogeneous and isotropic with parameters ε_2, μ_2. In either medium, the permittivities could be arbitrary and complex, and the permeabilities are considered to be that of free space: $\mu_1 = \mu_2 = \mu_0$.

Two analytical methods are developed for the solutions of the electric field induced internal to the tissue. The first method is based on the Lorentz theory[6] developed in the analysis of an artificial dielectric. Analytical expressions are obtained for the induced internal electric field. The second method uses an equivalent circuit approach. While the first method is more accurate, the solution of the second method, although admittedly approximate, is simpler to obtain and easier to understand. The numerical

calculations show good agreement between the results of these two methods. The calculated results for the internal electric field are graphically presented for certain lattice structures of the culture tray and for various geometric shapes of the object.

For the most part, the details of theoretical analysis are presented in the appendices, whereas the important results are summarized in the text of this report.

2. ANALYTICAL METHODS AND SOLUTIONS

As shown in Figure 1, the simulator for use in tissue culture experimentation employs parallel plates to generate an electric field, and a multi-coil to generate a magnetic field. The basic design requirement of this simulator is that it provides a uniform electromagnetic field over a desired test volume. A design goal was that variation of the field within the volume should not be more than 10 percent. Therefore, the impressed field considered in this study is assumed to be uniform. In addition, only the electric field coupling is considered, because the permeabilities of the biological objects and their surrounding medium are considered to be the same. Consequently, the magnetic field induced inside the object suffers no distortion or variation from the impressed magnetic field.

The electric field inside the object is induced by the impressed electric field. The tissue cultures which are embedded in the tissue culture tray for testing are exposed to the uniform electric field generated by the simulator. A sketch of the geometry is given in Figure 3. Because of the periodic arrangement of the tissue culture tray, the coupling mechanism is more complicated than that of a single isolated object. To determine the electric field strength internal to the object, we must take into account the interaction of the fields among all the objects. The solutions can be obtained from the interaction field approach presented below. A simple approximate method based on equivalent circuit technique is also given.

2.1 Interaction Field Approach-Lorentz Theory

When the interaction of a uniform electric field with a single isolated object is considered at extremely low frequencies, the coupling mechanism is essentially governed by the field boundary conditions. The coupling is stronger for objects having more elongated geometries. The biological tissue culture tray of Figure 3 considered here, however, is a large scale model of an actual dielectric obtained by arranging a number of identical biological tissues (objects) in a regular three-dimensional (or two-dimensional) pattern. Thus, the coupling mechanism becomes more complicated resulting from the interaction of the fields among all the objects. To take the interaction field into account, we note the Lorentz

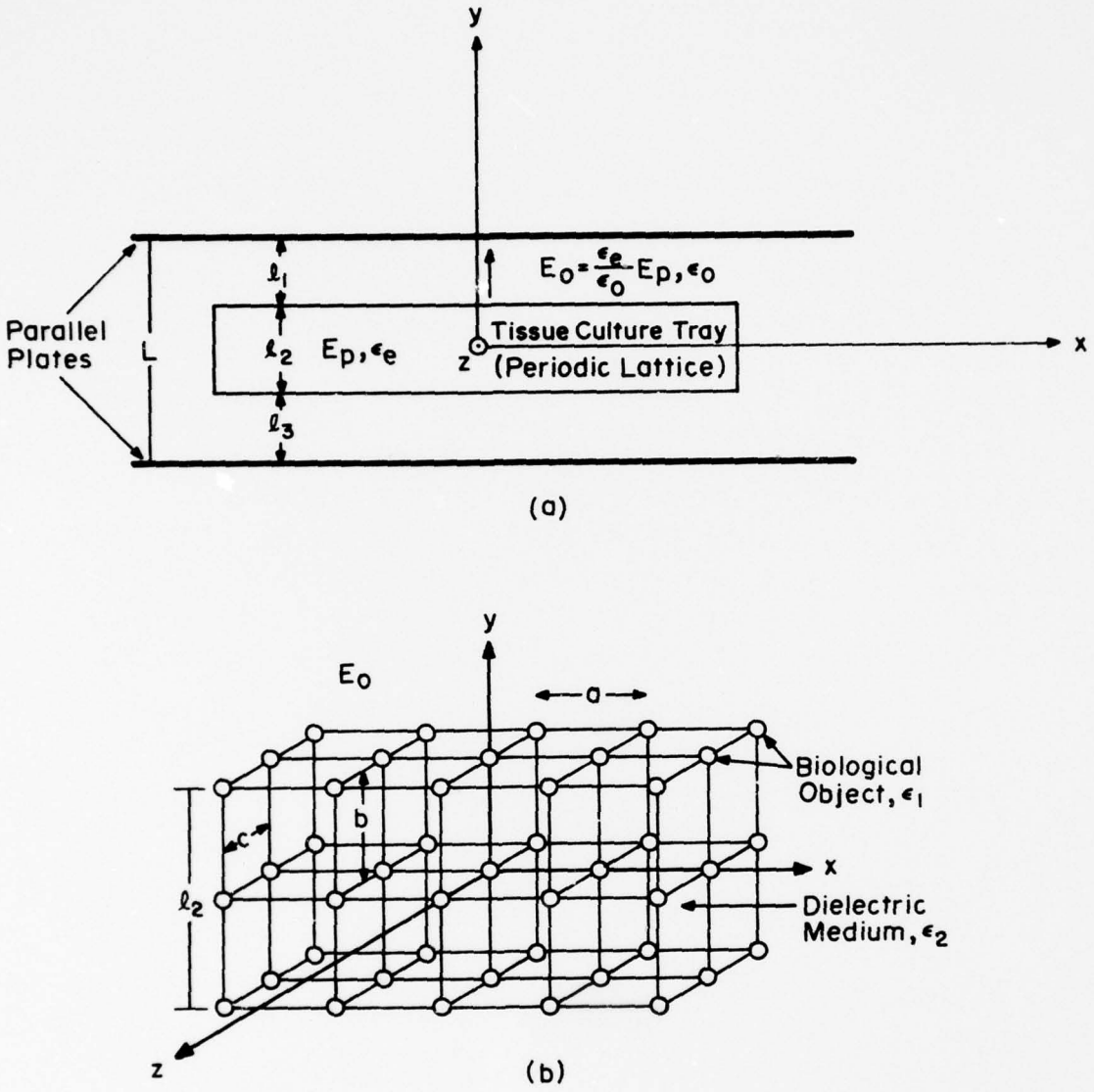

Fig. 3 BIOLOGICAL OBJECTS IN A PERIODIC LATTICE EXPOSED TO A UNIFORM ELECTRIC FIELD GENERATED BY THE SIMULATOR AT NMRI

theory which was originally developed for the theory of a dielectric.[6,7] This theory, which has been extensively used in the study of artificial dielectrics, considers dipole interactions among objects, and provides accurate results for object spacings limited to less than 0.1 of a wavelength and for object sizes small compared to a wavelength.

The electric field coupling to biological objects can be described, as Stratton[8] did, in terms of polarization (or dipole moment) because when exposed to a uniform electric field, electric charges are induced inside the object. These electric charges are displaced inside the objects so as to set up induced fields which will eventually satisfy the boundary conditions at the object surface. Since an electric dipole or simply a dipole is a name given to two point charges of equal magnitude but opposite sign separated by a small distance, the term polarization (or dipole moment) can be used to characterize the nature of biological objects under the influence of an impressed electric field. The ELF electric field coupling to dielectric objects of various geometric shapes is discussed in terms of polarization in Appendix A.

For the present problem, it is convenient to consider, without loss of any generality, that the biological tissues have their principal axes of polarization coincident with the coordinate axes (as shown in Figure 4) so that the induced dipole moment, p, of the object (tissue) is in the same direction as that of the impressed field. At extremely low frequencies, the field acting to polarize any object may be assumed to be a uniform field equal to the field at the center of the object. When each (biological) object is replaced by its equivalent dipole moment, p, (obtained from Appendix A), the tissue culture tray of Figure 3 considered here reduces to an equivalent dipole array. This equivalent dipole array is shown in Figure 4.

Since each object exhibits a dipole field, interaction occurs between objects. This interaction effect may be evaluated in terms of a constant, β, called the interaction constant which has been defined by Collin[6,9] in the work in connection with artificial dielectrics and aperture coupling in waveguides. The interaction constant for the present problem has been derived in Appendix B using the image theory for potential functions of either a three-dimensional array or a two-dimensional array.

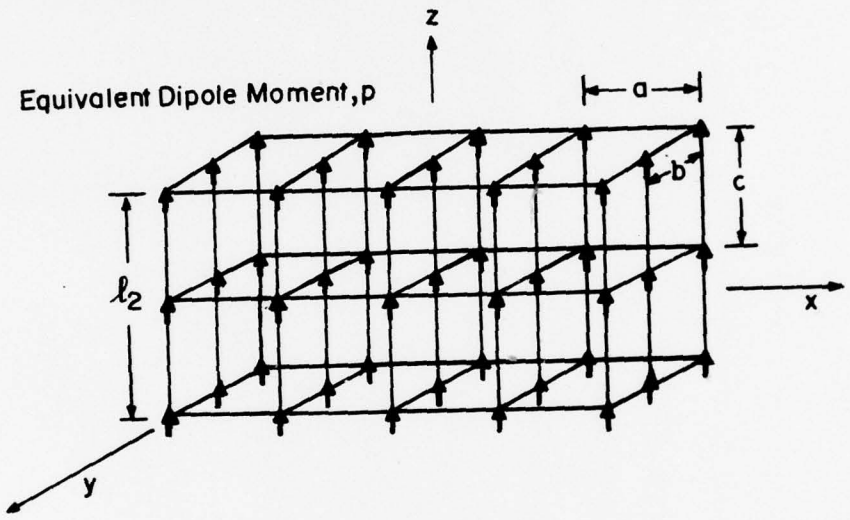

Fig. 4 AN EQUIVALENT DIPOLE ARRAY FOR THE PERIODIC LATTICE OF FIGURE 3.

As a result of this interaction, the net combined effect of all the objects is to produce a new average dipole moment at the center of each object. With the polarizability constant (Appendix A) and the interaction constant (Appendix B) obtained, the induced electric field, E_i, internal to the object under the influence of a uniform electric field may be obtained by using the concept of polarization and the theory of artificial dielectrics. The results obtained in Appendix C are

$$E_i = \left\{ \frac{\alpha_e/(\xi-1)}{(1-\alpha_e\beta)k_v} \right\} E_p \qquad (1)$$

where

$$E_p = \frac{V_o}{\{\ell_2 + (\varepsilon_e/\varepsilon_o)(\ell_1 + \ell_3)\}} \qquad (2)$$

$$\varepsilon_e = \varepsilon_2 \left\{ 1 + \frac{\alpha_e/abc}{(1-\alpha_e\beta)} \right\} \qquad (3)$$

In these expressions, the following parameters and notations are used.

a,b,c: object spacing along the direction of x,y,z axis, respectively, m.

$\ell_1(\ell_3)$: the spacing between the tissue culture tray and the upper (lower) plate of the simulator, m.

ℓ_2: thickness of the periodic lattice, m.

V_o: voltage applied between the parallel plates of the simulator, volts.

ε_o: free space permittivity, 8.854×10^{-12} farads/m.

ε_1: permittivity of the biological tissue, farads/m

ε_2: permittivity of the medium outside the biological tissue, farads/m.

ξ : $\varepsilon_1/\varepsilon_2$.

k_v: volume of the biological tissue, m^3.

α_e: polarizability constant (the polarizability constants for objects of various geometric shapes are listed in Table A-2 in Appendix A).

β: *interaction constant* (the interaction constants for the three-dimensional dipole array and the two-dimensional array are given in Equations (B-7) and (B-11) of Appendix B, respectively).

Using α_e and β obtained in Appendices A and B, Equations (1)-(3) can be used to calculate the induced electric field internal to the biological tissue, E_i. As an illustrative example, let us consider the biological objects having a prolate spheroid geometric shape. Using the expression of α_e listed in Table A-2 of Appendix A, it can be easily shown that Equations (1) and (3) become

$$E_i = \frac{\left(E_{p/\Delta}\right)}{\{1-k_v\beta(\xi-1)/\Delta\}} \tag{4}$$

$$\varepsilon_e = \varepsilon_2\left\{\frac{1+k_v(\xi-1)(abc-\beta)/\Delta}{1-k_v\beta(\xi-1)/\Delta}\right\} \tag{5}$$

respectively, where

$$\Delta = \{1+(\xi-1)(u^2-1)[u\coth^{-1}(u)-1]\} \tag{6}$$

$$u = \left[1-(r_b/r_a)^2\right]^{-1/2} \tag{7}$$

In Equations (4)-(7), r_a and r_b* denote the major and minor radius of the prolate spheroid, respectively, and E_p again is given by Equation (2).

This result indicates than when $\varepsilon_1 = \varepsilon_2$ (i.e., ξ=1), we have $\varepsilon_e = \varepsilon_2$ and $\Delta = 1$ which, in turn gives $E_i = V_o/[\ell_2 + (\varepsilon_2/\varepsilon_o)(\ell_1+\ell_3)]$. This result is identical to that obtained for a homogeneous dielectric slab situated between a parallel plate with an applied voltage V_o. It is also interesting to note that when r_b decreases, Δ decreases accordingly so that when $r_b = 0$, the result of E_i reduces to the result for a very thin and long cylindrical object. For $r_a/r_b = 1$, we find Δ approaches 1/3 and, hence, the result of E_i becomes that of a biological sphere.

*In Appendix A, the major and minor axes of the prolate (or oblate) spheroid are designated by a and b, respectively.

2.2 Circuit Approach

In this section, a simple circuit approach is discussed. While this method provides only approximate results, the solutions are useful for a quick estimate of the electric field induced inside the biological tissue and provide for an understanding of the coupling phenomenon.

As noted previously, the permittivities of the biological tissue and its surrounding medium could be complex. Denoting $\varepsilon_1 = \varepsilon_1' - j\varepsilon_1''$ and $\varepsilon_2 = \varepsilon_2' - j\varepsilon_2''$, the conductivities of the tissue and the medium are $\sigma_1 = \omega\varepsilon_1''$ and $\sigma_2 = \omega\varepsilon_2''$, respectively. Hence, the real part of the permittivity (ε_1' or ε_2'), like a capacitor represents the stored energy, and the imaginary part of the permittivity (ε_1'' or ε_2'') is responsible for the power loss. It can easily be seen that the tissue culture tray and the parallel plate simulator, shown in Figure 3, may be represented by an equivalent circuit obtained from an approximate geometric model. Two realistic geometric models which approximate the tissue culture tray of Figure 3 are illustrated in Figure 5, along with their corresponding equivalent circuits. The two geometric models presented here are considered to be illustrative and provide reasonably good approximations.

In the tissue culture tray, the medium which surrounds the biological tissue normally is a thin layer of perfect dielectric (i.e., $\varepsilon_2'' = 0$). Hence, the capacitor, C_o, is sufficient to characterize this medium. The same is true for the free space capacitor, C_1. The capacitance and resistance in the equivalent circuits can be obtained from

$$
\begin{aligned}
C_1 &= \frac{\varepsilon_o}{\ell_1} && \text{farads/m}^2 \\
C_o &= \frac{\varepsilon_2}{\ell_o} && \text{farads/m}^2 \\
R &= \frac{(\ell_2 - 2\ell_o)}{\sigma_1} && \text{ohm/m}^2 \\
R_2 &= \frac{(\ell_2 - 2\ell_o)}{\sigma_1 S_R} && \text{ohm/m}^2 \\
C_2 &= \left(\frac{\varepsilon_2}{\ell_2 - 2\ell_o}\right) S_C && \text{farads/m}^2
\end{aligned}
\qquad (8)
$$

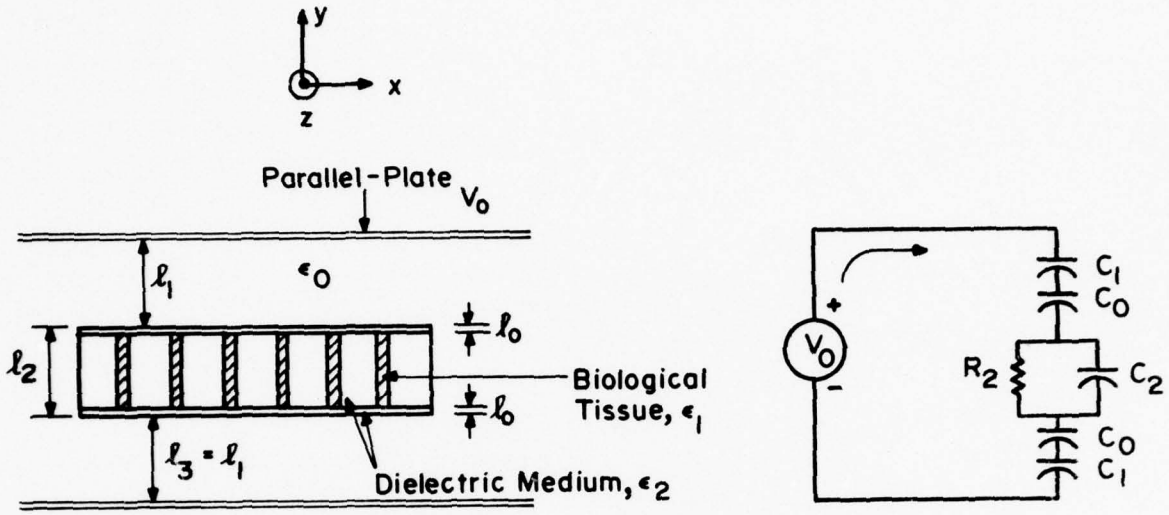

(a)

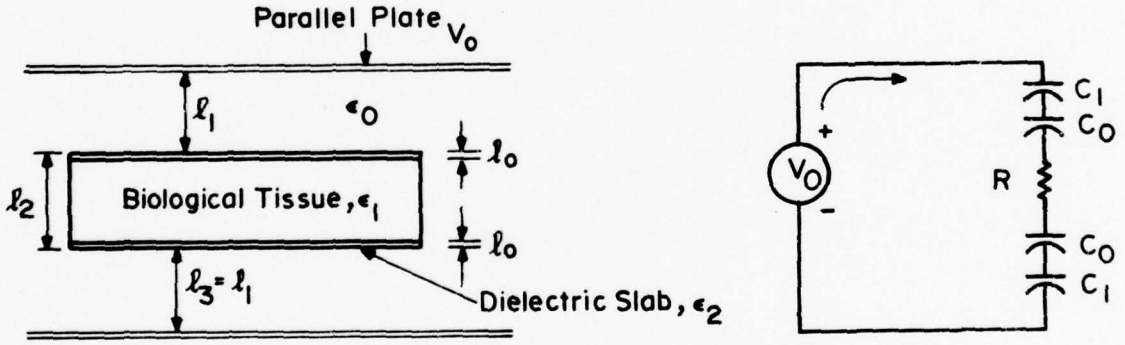

(b)

Fig. 5 APPROXIMATE GEOMETRIC MODELS FOR THE TISSUE CULTURE TRAY AND THEIR EQUIVALENT CIRCUITS

In Equation (8), we note that $S_R + S_C = 1$, where S_R is the ratio of the cross-sectional area of the tissue to that of the tissue culture tray in the x-z plane of Figure 5, and S_C denotes the ratio of the cross-sectional area occupied by the plastic (dielectric) to that of the tissue culture tray.

From these equivalent circuits, the voltage across the resistor of either R_2 (in Figure 5a) or R (in Figure 5b) can be obtained easily. If this voltage is V_R, then the electric field induced inside the biological tissue is $E_i = V_R/\ell_2$. On this basis, the equivalent circuit of Figure 5b is expected to yield a lower bound estimate of the field, E_i, since the flux would be uniform in this model. The equivalent circuit of Figure 5a will yield an upper bound estimate of E_i because it assumes that the flux captured by the tissue depends only on the cross-sectional area ratio.

3. CALCULATED RESULTS

Although the analysis presented in this study is generally applicable for calculating the induced electric field inside the biological tissue for any dimension of the simulator and for objects of any geometric shape, the calculations presented here emphasize the results obtained for the specific simulator and the tissue culture tray fabricated for the NMRI experiment. More parametric calculations are presented in Appendix C.

The simulator considered here generates ELF fields at a center frequency of 76 Hz. The complex permittivity of the biological tissue is considered to that of a high water content tissue. A search of available literature did not reveal an accurate value of the permittivity for the high water content biological tissue at extremely low frequencies. For higher frequencies above 1 kHz, the value of permittivity has been reported by Schwan[10] and Johnson and Guy.[11] Based on the extrapolation of their results for frequencies below 1 kHz, the realistic complex permittivity for a high water content biological tissue at extremely low frequencies (in the range from 45 Hz to 76 Hz) is considered to be approximately $\varepsilon_1 = \varepsilon_o(10^5 - j10^8)$ farads/m, where ε_o, the free space permittivity, is 8.854×10^{-12} farads/m. This value of ε_1 is used in the calculation.

To make the desired calculations, the following assumptions and parameters are used:

- The lattice spacings for the tissue culture tray of Figure 3 are measured to be 9.52, 15.08 and 9.52 mm along the x, y and z directions, respectively.
- In the tissue culture tray, the biological tissue is filled in a hollow cylindrical hole whose geometric shape resembles, to a certain degree, that of a prolate spheroid. Hence, the prolate spheroidal model of biological tissue is used in the calculation. For quantitative comparison, calculations are also made for spherical models of biological tissue.
- The biological tissue is embedded in a very thin layer of plastic (dielectric slab) with a zero loss tangent and a relative dielectric constant of 2.25 (i.e., $\varepsilon_2' = 2.25\ \varepsilon_o$ and $\varepsilon_2'' = 0$).

Using the prolate spheroidal model of biological tissue, the induced electric fields inside the tissue are calculated based on Equations (4)-(7). The major and minor radii of the prolate spheroid, r_a and r_b, are measured to be 6.35 mm and 3.18 mm, respectively. Figure 6 shows the calculated results for a two-dimensional array. In this case, the interaction constant, β, using the expression of Equation (B-11) is calculated to be $-2.25/\pi a^3$. The applied voltage between the parallel plates is taken to be 1 volt, and the results are plotted as a function of ℓ_1/ℓ_2 for two values of ℓ_2 and for the case of $\ell_1 = \ell_3$, where ℓ_2 is the thickness of the tissue culture tray and ℓ_1 (or ℓ_3) is the separation between the tray and the upper (or lower) plate of the simulator. Note that in this figure, only the magnitude of the field is given. Because of the strong capacitive effect associated with the tissue culture tray and the parallel plate, the induced internal electric field E_i and the applied voltage V_o are almost 90^o out of phase.

Figure 7 illustrates the corresponding results for the spherical model of biological tissue. The radius of the sphere, denoted by r_o,* is chosen to be about 4 mm such that the sphere has the same volume as that of the prolate spheroid.

Also of interest to the coupling problem is the three-dimensional lattice or array. When two or more two-dimensional tissue culture trays are stacked together, the structure becomes a three-dimensional array. Hence, for the same lattice spacings and object sizes, the three-dimensional culture tray would have a thickness ℓ_2, larger than that of a two-dimensional culture tray. Two values of ℓ_2, 75 mm and 150 mm, are used in the calculation. The results (using Equation (B-7) of Appendix B for the interaction constant, β) are graphically presented in Figures 8 and 9 for prolate spheroidal and spherical models of biological tissue, respectively.

---

*In Appendix A, the radius of a dielectric sphere is denoted by a.

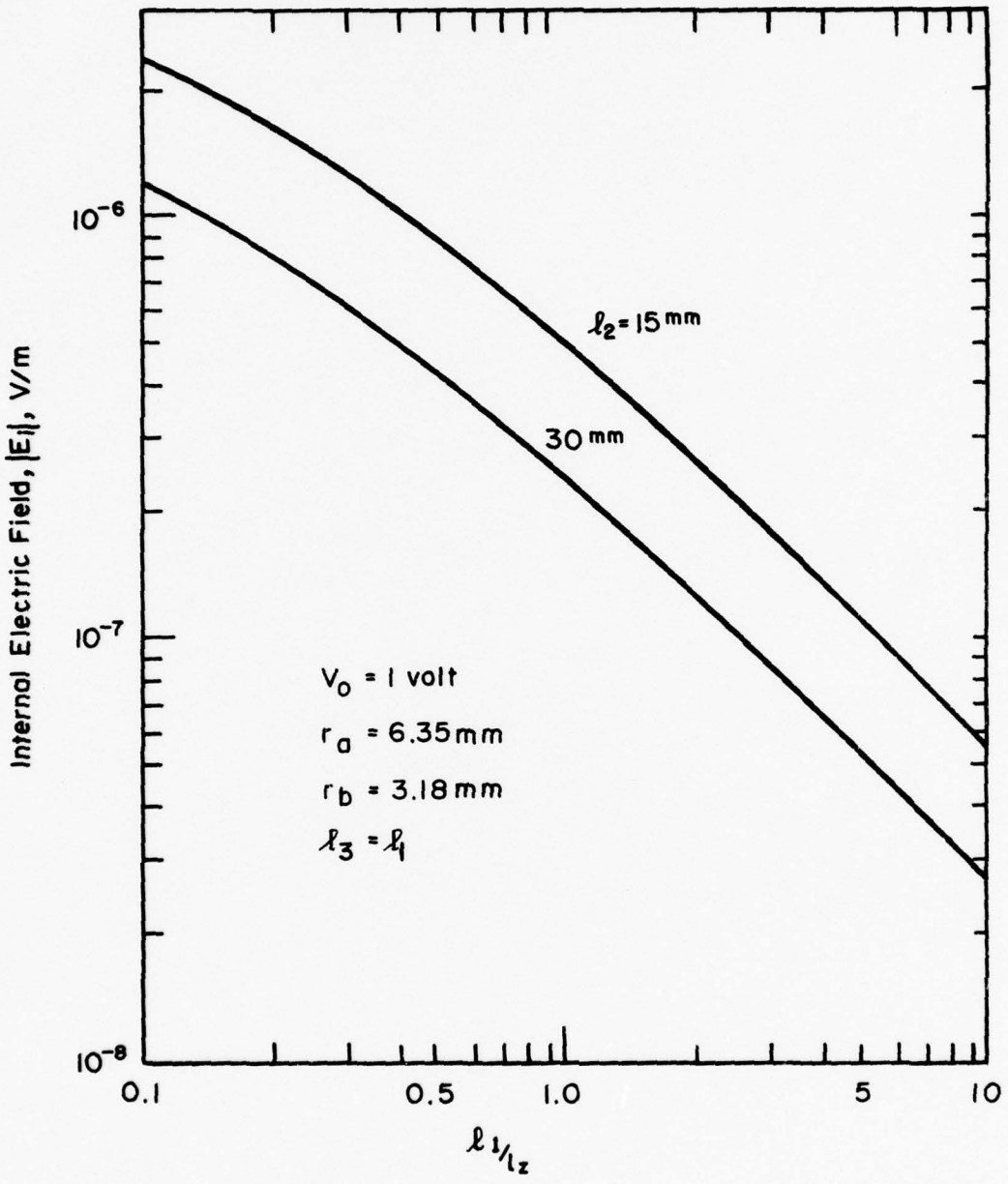

Fig. 6 INDUCED ELECTRIC FIELD INTERNAL TO THE PROLATE SPHEROIDAL MODEL OF BIOLOGICAL TISSUE IN A TWO-DIMENSIONAL TISSUE CULTURE TRAY

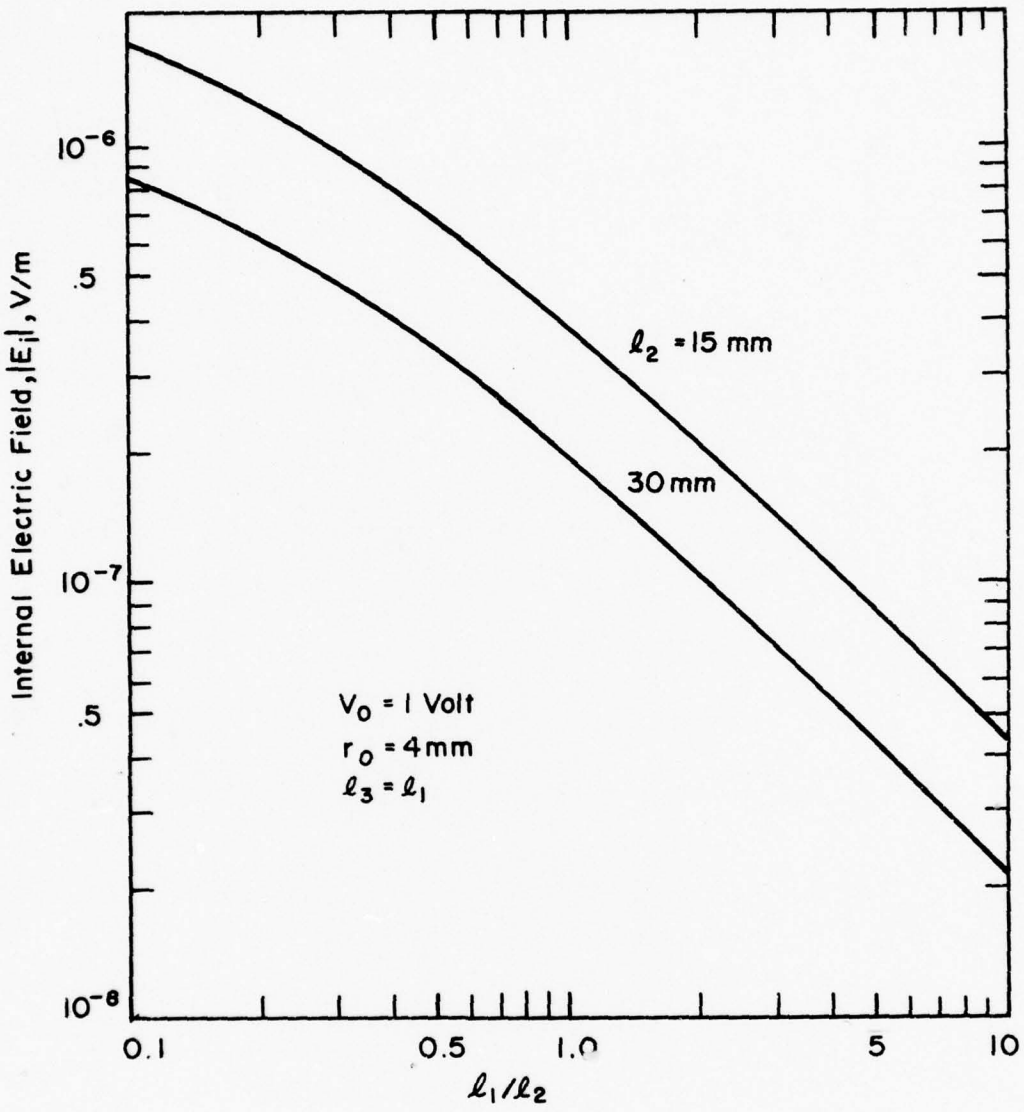

Fig. 7 INDUCED ELECTRIC FIELD INTERNAL TO THE SPHERICAL MODEL OF BIOLOGICAL TISSUE IN A TWO-DIMENSIONAL TISSUE CULTURE TRAY

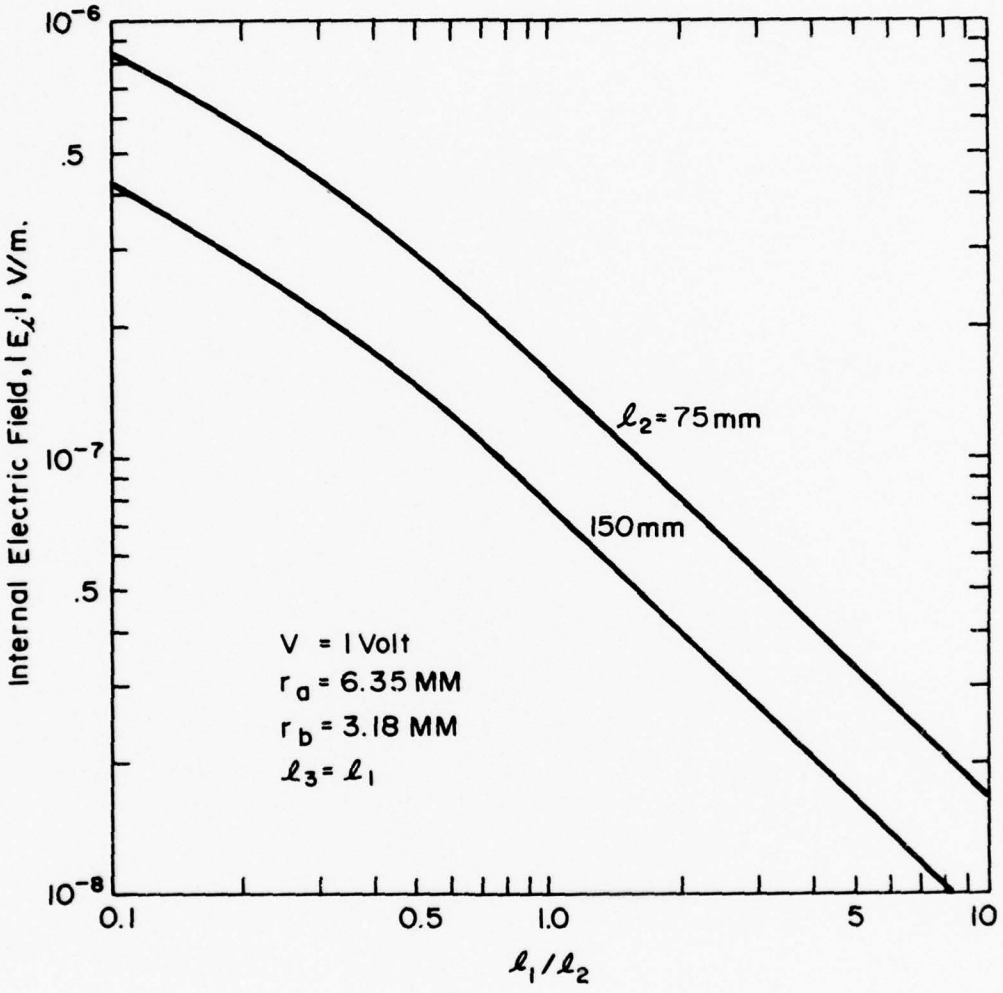

Fig. 8 INDUCED ELECTRIC FIELD INTERNAL TO THE PROLATE SPHERICAL MODEL OF BIOLOGICAL TISSUE IN A THREE-DIMENSIONAL TISSUE CULTURE TRAY

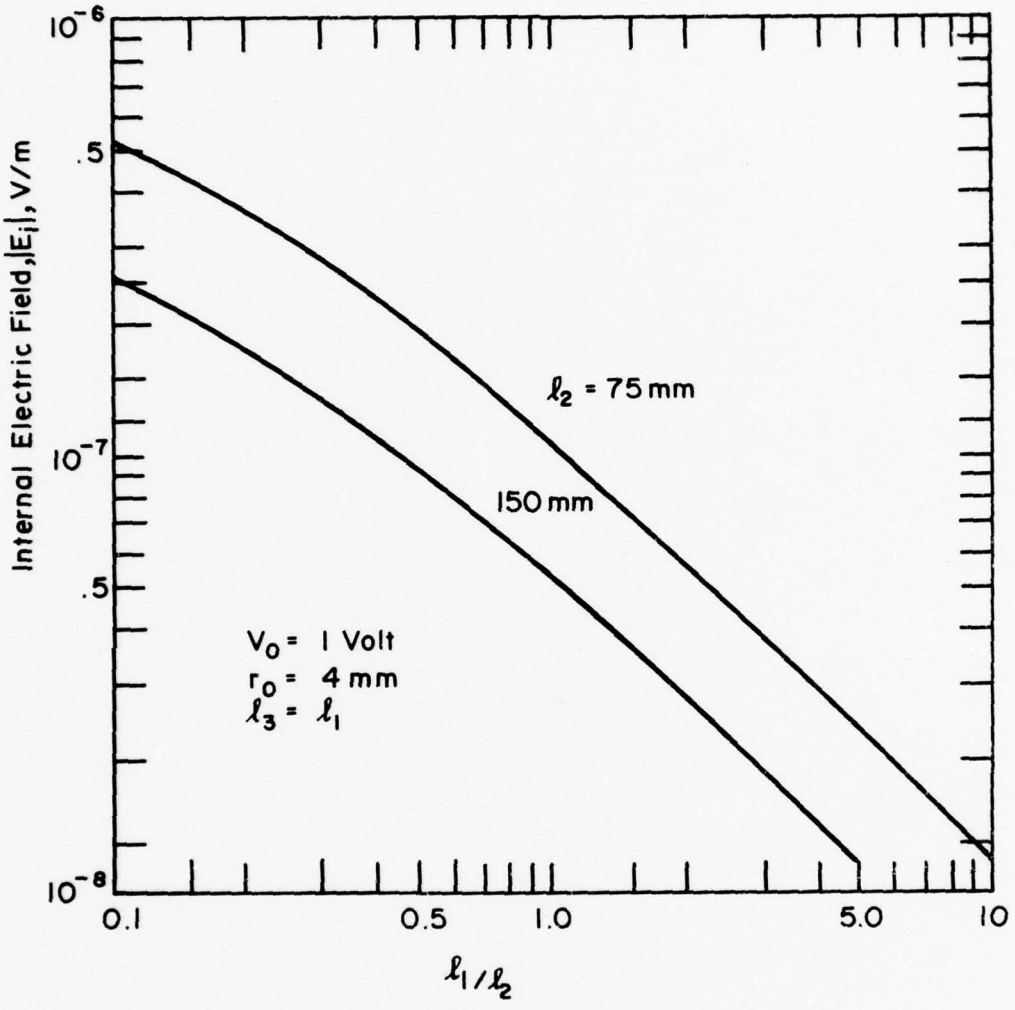

Fig. 9 INDUCED ELECTRIC FIELD INTERNAL TO THE SPHERICAL MODEL OF BIOLOGICAL TISSUE IN A THREE-DIMENSIONAL TISSUE CULTURE TRAY

Based on these data, we note that the induced electric field internal to the tissue culture decreases as ℓ_1/ℓ_2 increases. The maximum field strength occurs when the parallel plates are placed directly on the tissue culture tray. As anticipated, the coupling is stronger for a biological tissue sample (or object) having a more elongated geometric shape. When compared to the spherical model, the coupling is stronger for the prolate spheroidal model of the tissue sample. This is easily seen from the results presented in Figures 6 and 7.

To establish the validity of the analysis developed in this study, calculations using the circuit approach are also made. The results are compared with the more exact solutions, using the interaction field approach in Table 1. Note that the capacitor, C_2, in the equivalent circuit of Figure 5(a), in most practical situations, can be neglected without losing any accuracy in the result obtained. For example, the impedance of C_2 (i.e., $1/j\omega C_2$) is calculated to be $-j\ 1.62 \times 10^5$ ohms for the parameters and dimensions of present interest. When compared to resistance R_2, which is calculated to be about 32.5 ohms, the capacitor, C_2 may be ignored. The close agreement of the results between the two methods,

TABLE 1

ELF ELECTRIC FIELD COUPLING TO BIOLOGICAL TISSUE
UNDER NMRI SIMULATOR

Induced Internal Electric Field $\lvert E_i \rvert$ (V/m)*		
Rigorous Interaction Field Approach for a Two-Dimentional Periodic Array	Approximate Circuit Approach Using the Geometric Model of Figure 5(a)	Approximate Circuit Approach Using the Geometric Model of Figure 5(b)
1.17×10^{-7}	2.05×10^{-7}	0.71×10^{-7}

*ℓ_o = 1 mm, ℓ_2 = 15 mm, $\ell_1 = \ell_3$ = 70 mm

r_a = 6.35 mm, r_b = 3.18 mm

S_R = 0.349, S_C = 0.651

V_o = 1 volt.

as indicated in the Table, suggests that the solutions developed in this study can be used with confidence to calculate the induced electric field inside the tissue culture used in the NMRI experiment. It also indicates that the simple circuit approach, although admittedly approximate,provides a reasonable estimate. In fact, the results given in Table 1 for the geometric models of Figures 5(a) and 5(b) represent, respectively, the upper and lower bound values for the solution in question. The actual electric field that would be induced inside the tissue should have a value smaller than that predicted from the geometric model of Figure 5(a), but larger than that predicted from Figure 5(b).

Using the methods of Appendix A, it can be shown that for an external field of 20 V/m, the field internal to a biological body of permittivity $\varepsilon_1 = \varepsilon_o(10^5 - j10^8)$ would be approximately 6×10^{-7} V/m. To develop this field in tissue samples in a plastic tray like the one shown in Figure 2, requires 5.2 volts across the plates of the simulator for the present plate spacing (approximately 6 inches). This is for a single layer of trays. For five layers of trays, 2.1 volts is required. These calculations were made using the equations and graphs of Sections 2 and 3. Linear interpolation may be used to determine the required voltage across the plates for a number of layers of trays between one and five.

The tissue samples near the edges of the trays will experience somewhat stronger exposure than the rest of the array. This has not been quantified further.

4. SUMMARY AND CONCLUSIONS

The Naval Medical Research Institute (NMRI) is performing an experiment to study the possible effects of the electric and magnetic fields associated with the Navy's proposed ELF Communications System (Seafarer) on human tissue cultures. This report presents the results of a supporting study of the electric field coupling to the tissue culture samples.

Two analytical methods are developed in this study. The first method, which considers the dipole field interaction, is more accurate. The second method is very simple, using an approximate equivalent circuit treatment. The agreement of the results obtained from these two methods is fairly good. Therefore, the resultant expressions can be used with confidence in the studies of ELF electric field coupling to biological tissue and in many problem areas concerning the electromagnetic biological effects.

Observations and conclusions drawn from this study are:

(1) The ELF magnetic field will penetrate the tissue cultures without change.

(2) As anticipated, the induced electric field internal to the biological tissue in the tissue culture tray decreases as the permittivities of the tissue and its surrounding medium increases.

(3) The ELF electric field internal to the tissue sample will be much less than the applied field. For a single layer of trays, the reduction factor is about 6×10^7.

(4) The electric field coupling to the tissue also depends upon the separation between the tissue culture tray and the upper and lower plates of the simulator. Maximum internal field strength is achieved when the parallel plates are placed right on and beneath the culture tray.

(5) Like the ELF electric field coupling to a single isolated biological object, the coupling is stronger for objects having a more elongated geometric shape. The coupling is strong when the object exhibits a geometric shape somewhat like a long and thin circular cylinder. On the other hand, the coupling is small for geometric shape somewhat like a flat circular disk.

(6) From the limited numerical results obtained in this study (see Appendix C), it appears that the array spacing and the object size also affect the electric field coupling. However, the effect, which primarily arises from the variation in the effective permittivity of the tissue culture tray for different array spacing and object size, is not significant at extremely low frequencies.

(7) Although sophisticated field theory has been required to analyze the complex geometry used in this experiment, an adequate estimate of the field coupling can be obtained using a simple circuit model. This model also aids in the understanding of the coupling mechanism.

APPENDIX A

ELF ELECTRIC FIELD COUPLING TO DIELECTRIC OBJECTS OF SIMPLE GEOMETRIC SHAPE

1. INTRODUCTION

The electric field coupling to and penetration of dielectric objects depends on the frequency of the electric field, the complex permittivity (i.e., the dielectric constant and conductivity) of the object and its surrounding medium, and the size and shape of the object. At extremely low frequencies (ELF) the simplifying assumption is made that the object is small compared to wavelength and then only the shape of the object and the permittivities involved are parameters. Of interest are the electric field internal to the object, E_i, the polarization, P, and the polarizability, α_e, of the object.

The simple geometric shapes to be considered here are illustrated in Figure A-1. The cylinders of Figures A-1(b) and A-1(c) are assumed to be very thin and the slab of Figure A-1(d) is also assumed to be very thin. The prolate (or oblate) spheroid is formed by the rotation of an ellipse about its major (or minor) axis. In each case the permittivity of the outside medium is designated ε_2 and that of the inside medium is ε_1. These permittivities are complex. For example,

$$\varepsilon_1 = \varepsilon_1' - j\varepsilon_1'' \qquad \text{(A-1)}$$

where

ε_1' = permittivity

$\varepsilon_1'' = \dfrac{\sigma_1}{\omega}$

σ_1 = conductivity

$\omega = 2\pi f$

f = frequency.

2. INTERNAL ELECTRIC FIELD

The induced field within the dielectric object when exposed to an ELF electric field may be obtained for the simple geometric shapes of Figure A-1. The results are presented in Table A-1.

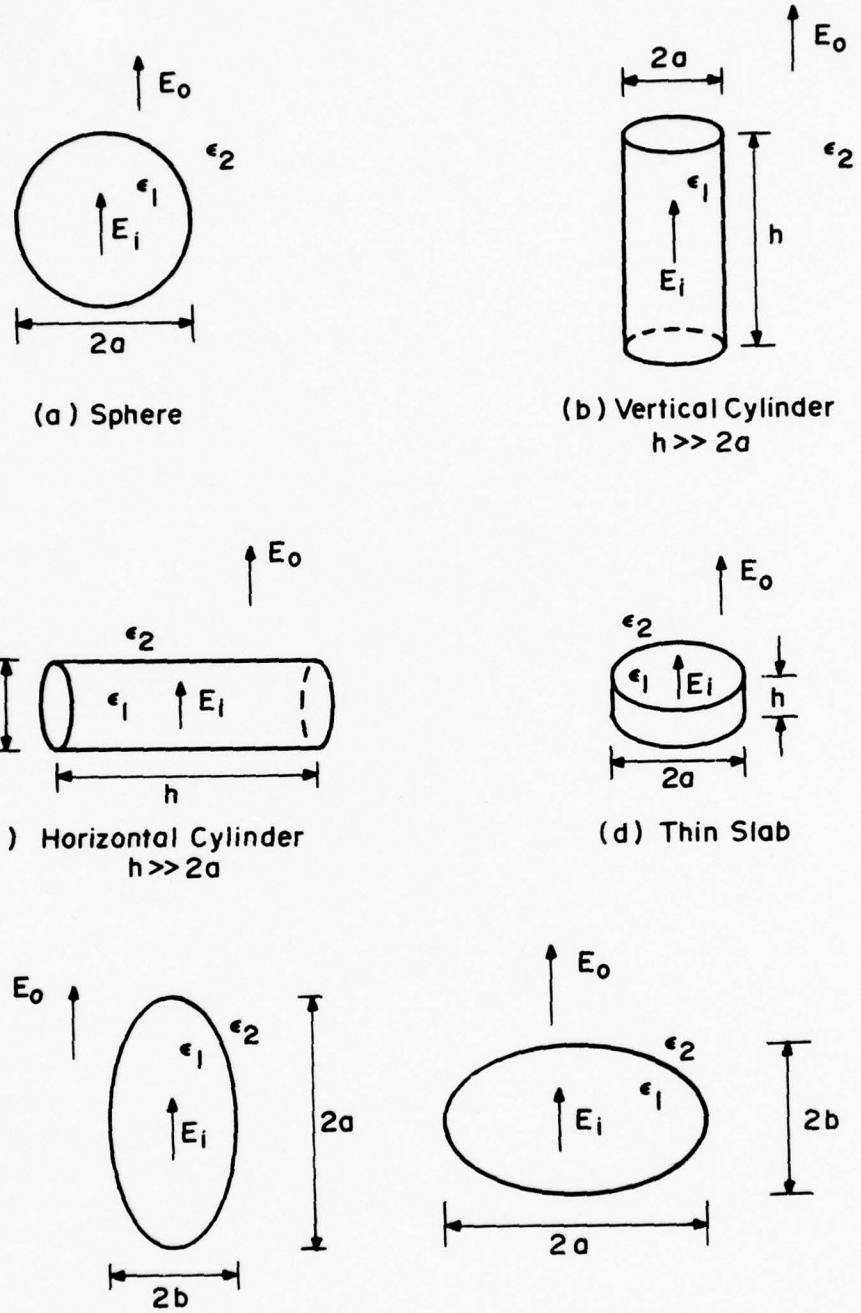

Fig. A-1 DIELECTRIC OBJECTS OF SIMPLE GEOMETRIC SHAPE

The static solution for a dielectric sphere has been obtained by Stratton[8] (pp 205-206). The sphere has been used by many investigators as an approximate geometric model for human baby.[12,13] Note that the internal field is polarized along the same direction as the electric field impressed on the object. The internal field is uniform and is independent of sphere size.

For the long thin cylinder of Figure A-1(b) with impressed electric field along its axis, the continuity of the tangential electric field along the surface boundary requires that $E_i \approx E_o$. Again, this approximation is independent of the cross-sectional shape of the cylinder and is valid when the cylinder is long and thin.

In Figure A-1(c), the external electric field is normal to the axis of the thin cylinder. The result given in Table A-1 is the static solution obtained by Smyth.[14]

For the thin slab with the electric field normal to it, the continuity of the normal component of electric flux requires that $\varepsilon_2 E_o = \varepsilon_1 E_i$.

The prolate spheroid shown in Figure A-1(e) is a symmetric ellipsoid which is generated by revolving an ellipse about its major axis. The oblate spheroid, as shown in Figure A-1(f), is formed by the revolution of an ellipse about its minor axis. A very general static solution for the case of an ellipsoid has been developed by Stratton[8] (pp 211-213), but the resultant expression is in terms of elliptical integrals which usually require approximate numerical treatment. A conclusion of great practical importance that can be reached from Stratton's results is that if the applied field is initially uniform and parallel to one of the ellipsoid axes, then the resultant internal field within the ellipsoid is also uniform and parallel to that same axis. In Table A-1, we list the solutions for the prolate spheroid and the oblate spheroid. These low frequency results are obtained for these two non-spherical spheroids using the method of separation of variables.[15] The parameters u and $\bar{u}$ for the prolate spheroid and the oblate spheroid are given by

Table A-1

INDUCED INTERNAL FIELDS FOR DIELECTRIC OBJECTS
OF SIMPLE GEOMETRIC SHAPES

Geometric Shape	Sphere Figure A-1(a)	Thin Vertical Cylinder Figure A-1(b)	Thin Horizontal Cylinder Figure A-1(c)	Thin Slab Figure A-1(d)	Prolate Spheroid Figure A-1(e)	Oblate Spheroid Figure A-1(f)
Induced internal field, E_i, for a uniform outside field, E_o.	$\frac{3\varepsilon_2}{\varepsilon_1 + 2\varepsilon_2} E_o$	E_o	$\frac{2\varepsilon_2}{\varepsilon_1 + 2\varepsilon_2} E_o$	$\frac{\varepsilon_2}{\varepsilon_1} E_o$	$\frac{E_o}{\left\{1 + \left(\frac{\varepsilon_1}{\varepsilon_2} - 1\right)(u^2 - 1)\left[u \coth^{-1}(u) - 1\right]\right\}}$ $u = \left[1 - \left(\frac{b}{a}\right)^2\right]^{-1/2}$	$\frac{E_o}{\left\{1 + \left(\frac{\varepsilon_1}{\varepsilon_2} - 1\right)(\bar{u}^2 + 1)\left[1 - \bar{u} \cot^{-1}(\bar{u})\right]\right\}}$ $\bar{u} = \left(\frac{b}{a}\right)\left[1 - \frac{b}{a}^2\right]^{-1/2}$

$$u = \left[1-\left(\frac{b}{a}\right)^2\right]^{-1/2}$$

$$\bar{u} = \left(\frac{b}{a}\right)\Big/\left[1-\left(\frac{b}{a}\right)^2\right]^{-1/2} \qquad \text{(A-2)}$$

where 2a and 2b are the major and minor axes of the spheroid, respectively. Since the limit as $b \to a$ corresponds to the limit of $u \to \infty$ (or $\bar{u} \to \infty$), it can be shown that under this limiting case, the induced internal electric field becomes $E_i = 3E_o/(\varepsilon_1/\varepsilon_2+2)$ for both prolate and oblate spheroids. As expected, this is identical to the solution obtained for a dielectric spheroid.

The field boundary conditions require the magnitude of the tangential internal electric field to approach that of the tangential external field. The field boundary conditions also require the normal component of the internal field to be that of external fields reduced by a factor of $\varepsilon_2/\varepsilon_1$ which, in general, is a small quantity. Hence, as can be seen from Table A-1, the coupling of ELF electric field into the object is the strongest for the very thin cylinder as shown in Figure A-1(b), because the incident electric field is tangential to most of its surface boundary. For the prolate spheroid of Figure A-1(e), the incident electric field is tangential to the long major axis of the spheroid. Thus, the electric field coupled into the prolate spheroid is the next strongest. When compared to prolate spheroid, the oblate spheroid provides a weaker coupling, because for the same b/a ratio, the prolate spheroid represents a more elongated geometry than the oblate spheroid. For the symmetric dielectric sphere, the internal induced field strength is smaller than that of a prolate spheroid, but is larger than the field coupled into an oblate spheroid. The geometry of a horizontal circular cylinder can provide a relatively small electric field coupling, but the coupling is the smallest for the thin slab of Figure A-1(d), because the external impressed field is perpendicular to most of its surface boundary. This demonstrates that the ELF electric field coupling to dielectric objects is strongly dependent on the geometric shape of the object, but not dependent on the size of the object which is much smaller than wavelength at extremely low frequencies.

3. POLARIZATION AND POLARIZABILITY CONSTANT OF DIELECTRIC OBJECTS

A characteristic of all dielectric materials is their ability to store electric energy under the influence of an electric field. This storage of energy takes place by a shift in the relative positions of the internal positive and negative charges against normal molecular and atomic forces. Under the influence of a given electric field, the amount of the charge displacement differs for different dielectric materials. Electrical dipole or simply a dipole is the name given to two point charges of equal magnitude and opposite sign separated by a small distance. The term "polarization" or (dipole moment) is used to characterize the nature of dielectric material and its geometric shape when exposed to an external electric field.

Consider a dielectric object embedded in a homogeneous and isotropic medium. The permittivities of the dielectric object and its surrounding medium are designated by ε_1 and ε_2, respectively. Under the influence of a uniform external field, E_o, the polarization of the object, p, defined by Stratton[8] (pp 183 and 206) is given by

$$P = (\varepsilon_1 - \varepsilon_2)\, E_i \qquad \text{(A-3)}$$

As illustrated in Table 1, the internal induced field, E_i, is related to the external field E_o. Hence, the polarization of a dielectric object can be expressed in terms of the external field, E_o. As an example, the polarization of a dielectric sphere, from Equation (A-3), is

$$P = 3\varepsilon_1 \left(\frac{\varepsilon_1 - \varepsilon_2}{\varepsilon_1 + 2\varepsilon_2} \right) E_o \qquad \text{(A-4)}$$

Since the polarization is also defined as the dipole moment, p, per unit volume, Equation (A-4) gives

$$p = 4\pi a^3\, \varepsilon_1 \left(\frac{\varepsilon_1 - \varepsilon_2}{\varepsilon_1 + 2\varepsilon_2} \right) E_o \qquad \text{(A-5)}$$

The relationship between polarization P (or dipole moment p) and the impressed external field, E_o, is, of course, a function of the type of dielectric material. For isotropic material which is the case of present interest, P (or p) and E_o are linear related and are always parallel regardless of the orientation of the external field. The constant which characterizes this relationship between p and E_o is termed the polarizability, α_e, of the dielectric object.

$$p = \alpha_e \varepsilon_2 E_o \tag{A-6}$$

To illustrate this, consider the dielectric sphere of Figure A-1(a). A comparison between Equations (A-5) and (A-6) gives the polarizability constant for the dielectric sphere

$$\alpha_e = 4\pi a^3 \left(\frac{\xi-1}{\xi+2}\right) \tag{A-7}$$

where $\xi = \varepsilon_1/\varepsilon_2$

Figure A-2 illustrates the polarizability for a dielectric sphere with a real permittivity (i.e., $\varepsilon_1'' = 0$). In the figure, the polarizability, α_e, is normalized to $4\pi a^3$, where a is the radius of the sphere. It can be seen that α_e becomes zero if ξ is taken to be unity. This is expected because when $\varepsilon_1 = \varepsilon_2$ no dielectric object exists in the medium. It is also of interest to consider the case of perfect conducting objects. Noting that the conductivity of a dielectric sphere with a complex permittivity $\varepsilon_1' - j\varepsilon_1''$ is given by $\sigma_1 = \omega\varepsilon_1''$, a dielectric object with ε_1'' approaching ∞ would be equivalent to a perfect conducting body. The polarizability of Equation (A-7) under this limiting case of $\varepsilon_1'' \to \infty$ gives $\alpha_2 = 4\pi a^3$, the polarizability of a conducting sphere. This result agrees with those used in the theory of artificial dielectric.[6,7]

Using Equations (A-3) and (A-6) the polarization P and the polarizability α_e for the dielectric objects of Figure A-1 can be obtained. The resultant expressions are summarized in Table A-2. These simple expressions are useful in studies of artificial dielectric, waveguide array and the interaction field of dielectric objects in a periodic lattice.

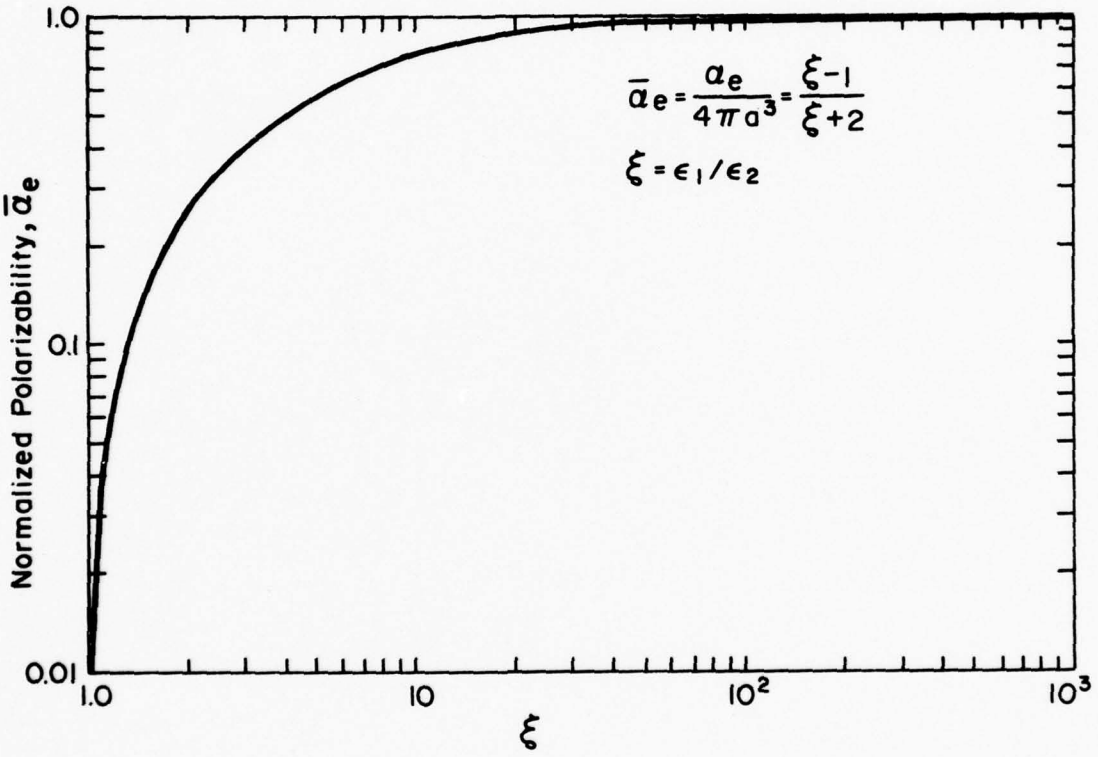

Fig. A-2 POLARIZABILITY OF A DIELECTRIC SPHERE

Table A-2

POLARIZATION AND POLARIZABILITY CONSTANT
FOR DIELECTRIC OBJECTS OF SIMPLE GEOMETRIC SHAPES

Geometric Shapes	Sphere Figure A-1(a)	Thin Vertical Cylinder Figure A-1(b)	Thin Horizontal Cylinder Figure A-1(c)	Thin Slab Figure A-1(d)	Prolate Spheroid Figure A-1(e)	Oblate Spheroid Figure A-1(f)
Polarization, P	$3\left(\frac{\varepsilon_1-\varepsilon_2}{\varepsilon_1+2\varepsilon_2}\right)\varepsilon_2 E_o$	$(\varepsilon_1-\varepsilon_2)\, E_o$	$2\left(\frac{\varepsilon_1-\varepsilon_2}{\varepsilon_1+\varepsilon_2}\right)\varepsilon_2 E_o$	$\left(\frac{\varepsilon_1-\varepsilon_2}{\varepsilon_1}\right)\varepsilon_2 E_o$	$\frac{(\varepsilon_1-\varepsilon_2)\, E_o}{\left\{1+\left(\frac{\varepsilon_1}{\varepsilon_2}-1\right)(u^2-1)\left[u\coth^{-1}(u)-1\right]\right\}}$	$\frac{(\varepsilon_1-\varepsilon_2)\, E_o}{\left\{1+\left(\frac{\varepsilon_1}{\varepsilon_2}-1\right)(\bar{u}^2-1)\left[1-\bar{u}\cot^{-1}(\bar{u})\right]\right\}}$
Polarizability Constant, α_e	$4\pi a^3\left(\frac{\xi-1}{\xi-2}\right)^*$	$\pi a^2 h(\xi-1)$	$2\pi a^2 h\left(\frac{\xi-1}{\xi+1}\right)$	$\pi a^2 h\left(\frac{\xi-1}{\xi}\right)$	$\frac{\frac{4}{3}\pi a b^2(\xi-1)}{\left\{1+(\xi-1)(u^2-1)\left[u\coth^{-1}(u)-1\right]\right\}}$ $u=\left[1+\left(\frac{b}{a}\right)^2\right]^{-1/2}$	$\frac{\frac{4}{3}\pi a b^2(\xi-1)}{\left\{1+(\xi-1)(\bar{u}^2+1)\left[1-\bar{u}\cot^{-1}(\bar{u})\right]\right\}}$ $\bar{u}=\left(\frac{b}{a}\right)\left[1-\left(\frac{b}{a}\right)^2\right]^{-1/2}$

*$\xi = \varepsilon_1/\varepsilon_2$

APPENDIX B

STATIC INTERACTION FIELDS IN A PERIODIC LATTICE

1. INTRODUCTION

The electric field coupling to dielectric objects can be discussed in terms of polarization (or dipole moment), because, under the influence of an external field, charges are induced in the object and are displaced so as to set up an induced field that will eventually satisfy the boundary conditions on the dielectric surface. Each dielectric object generates a dipole field and, thus, exhibits a dipole moment. When a great number of dielectric objects are embedded in a homogeneous and isotropic medium, interaction occurs between all of the dipole fields produced by the objects. In this Appendix, a suitable analytical method is presented to determine the interaction fields for the dielectric objects in a periodic lattice. Of present interest is the interaction of electric fields at extremely low frequencies (ELF). However, the results can be easily extended to include the magnetic field coupling and the case of plane electromagnetic fields.

2. INTERACTION FIELDS FOR DIELECTRIC OBJECTS IN A THREE-DIMENSIONAL PERIODIC LATTICE

The periodic lattice considered here is shown in Figure B-1, where the spacings between objects are designated by a, b, and c along the x, y, and z axes, respectively. At extremely low frequencies, only the static interaction field is of interest, because the size of the object and the spacings between the objects are sufficiently small compared to wavelength.

To obtain the static interaction field for the lattice of Figure B-1, each dielectric object may be represented by its equivalent dipole moment, p. The dipole moment (and the electric field coupling) for dielectric objects of simple geometric shapes has been discussed in Appendix A. For objects that are symmetrically distributed, the image theory of perfect conducting planes may be employed. It can be seen from Figure B-1 that conducting planes may be inserted into the lattice structure at $y = \pm b/2$ without disturbing the field distribution. Hence, by using image theory, the potential distribution of the lattice of Figure B-1 may be obtained by first considering the potential for a y-directed dipole located at $y = 0$ between the conducting plates at $y = \pm b/2$ as shown in Figure B-2, and then summing the potential distributions for all the dipoles placed at $x = na$, $y = 0$ and $z = sc$ for $n = 0, \pm 1, \pm 2 \cdots$ and $s = 0, \pm 1, \pm 2 \cdots$.

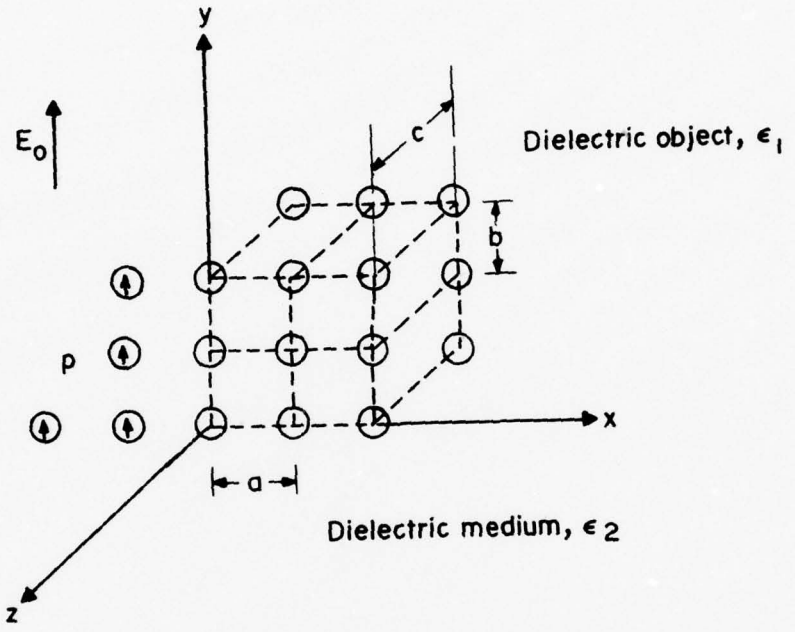

Fig. B-1. DIELECTRIC OBJECTS IN A THREE-DIMENSIONAL PERIODIC LATTICE

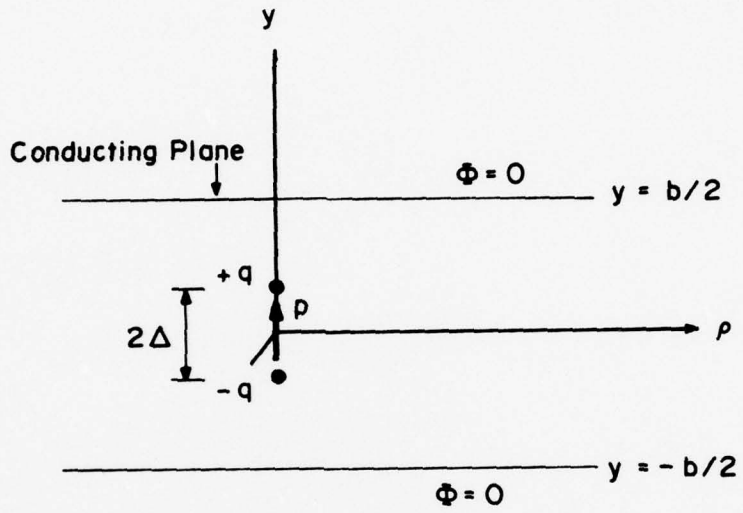

Fig. B-2 POTENTIAL DISTRIBUTION FOR AN ELECTRIC DIPOLE BETWEEN TWO CONDUCTING PLATES

The dipole at the origin may be considered as a positive charge $q\,\delta(x)\,\delta(z)\,\delta(y-\Delta)$ at $x = z = 0$, $y = \Delta$ and a negative charge $-q\,\delta(x)\,\delta(z)\,\delta(y+\Delta)$ at $x = z = 0$, $y = -\Delta$, where $\delta(x-x_0)$ represents the delta function which is defined to be equal to zero at all points of x except at $x = x_0$ where it becomes infinite. The potential function for the lattice of Figure B-2 is governed by the static Poisson's equation which in cylindrical coordinates (ρ,θ,y) is given by

$$\frac{\partial^2\Phi}{\partial y^2} + \frac{1}{\rho}\frac{\partial}{\partial\rho}\left(\rho\frac{\partial\Phi}{\partial\rho}\right) = -\frac{q}{\varepsilon_2}\,\delta(x)\delta(z)\left[\delta(y-\Delta)-\delta(y+\Delta)\right] \qquad \text{(B-1)}$$

The solution of Equation (B-1) has been obtained by Collin[9] and the resultant expression is given by Equation (B-3) below. The mathematical treatment is briefly presented as follows.

The potential function Φ is independent of θ. It can also be seen from Figure B-2 that Φ is an add function of y and must vanish on the conducting planes at $y = \pm b/2$. The solutions of Equation (B-1) having a variation of $\sin(2m\pi y/b)$ with respect to y, are the functions of the modified Bessel functions of the first and second kind. Only the second kind of the modified Bessel function $K_0(2m\pi\rho/b)$ is allowed, because it satisfies the radiation condition that $\Phi \to 0$ as $\rho = (x^2+z^2)^{1/2}$ becomes large. Hence, the general solution for the potential function Φ may be expressed as

$$\Phi(y,\rho) = \sum_{m=1}^{\infty} Am\,\sin\left(\frac{2m\pi y}{b}\right)\,K_0\left(\frac{2m\pi\rho}{b}\right) \qquad \text{(B-2)}$$

where the constant Am is determined from the dipole source as $\rho \to 0$. Noting that the dipole moment p is defined as $p = 2q\Delta$ as Δ approaches zero, the constant Am is $2mp/\varepsilon_2 b^2$, where ε_2 is the permittivity of the medium in which dielectric objects are embedded. Summing up the potential distributions due to the dipoles along the x and z axes and noting that the electric field is related to the potential function by $E = -\partial\Phi/\partial y$, the resultant expression for the interaction field due to all dipoles including the one at the origin is given by

$$E_{yi} = \frac{p}{\pi\varepsilon_2}\left\{\sum_{m=1}^{\infty}\left(\frac{1}{mb}\right)^3 - \frac{1}{b}\sum_{m=-\infty}^{\infty}{}'\sum_{n=\infty}^{\infty}\sum_{s=-\infty}^{\infty}\left(\frac{2m\pi}{b}\right)K_o\left(\frac{2m\pi}{b}\left[(na)^2+(sc)^2\right]^{1/2}\right)\right\}\cos\left(\frac{2m\pi y}{b}\right) \quad \text{(B-3)}$$

where the prime in the summation over m indicates the omission of the term $m = n = s = 0$.

The modified Bessel function of the second kind, $K_o(x)$, has the property that as x increases, $K_o(x)$ decreases rapidly. This is evidenced from Figure B-3 in which $K_o(x)$ is plotted as a function of x. Using the fact that $K_o(x)$ decays exponentially at a rapid rate and that[16]

$$\sum_{m=1}^{\infty}\left(\frac{1}{mb}\right)^3 = \frac{1.201}{b^3} \quad \text{(B-4)}$$

the interaction field at the center of the dielectric object (at y=0), from Equation (B-3), may be approximated by the following simple form

$$E_{yi} \approx \frac{p}{\varepsilon_2 b^3}\left\{\frac{1.201}{\pi} - 8\pi\left[K_o\left(\frac{2\pi c}{b}\right) + K_o\left(\frac{2\pi a}{b}\right)\right]\right\} \quad \text{(B-5)}$$

In most cases, Equation (B-5) provides sufficient accuracy for the solution, especially when a and c do not differ greatly from b. A simple numerical computation indicates that, if a = b = c, the calculated value for the largest term neglected in Equation (B-5) is less than 0.2 percent that of the second term of Equation (B-5). The expression of Equation (B-5) represents the interaction field at the center of the dielectric object arising from the interaction of all the dipole fields generated in the periodic lattice.

The relationship between the interaction field, Ey_i, and the dipole moment of a single (isolated) dielectric object is linear, as is clearly

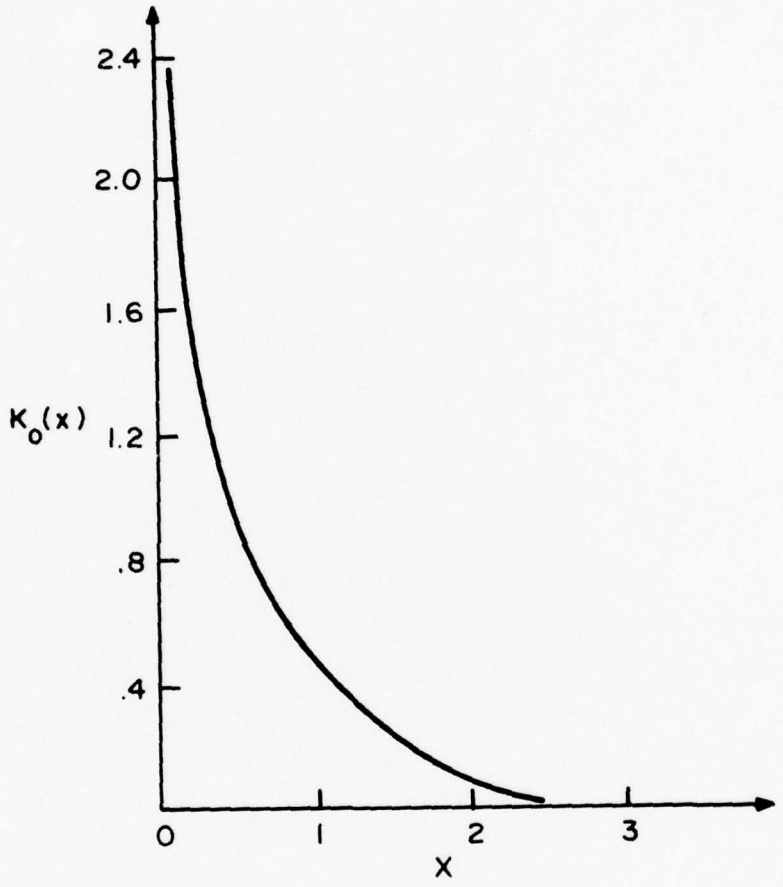

Fig. B-3 MODIFIED BESSEL FUNCTION OF THE SECOND KIND

indicated from Equation (B-5). The constant which characterizes this relationship is the interaction constant. The interaction constant, defined as [6,9]

$$\beta = E_{yi}\left(\frac{\varepsilon_2}{p}\right) \tag{B-6}$$

has been extensively used in the theory of artificial dielectrics. From Equations (B-5) and (B-6), the interaction constant, β, for the three-dimensional periodic lattice of Figure 1 is given by

$$\beta \approx \frac{1}{b^3}\left\{\frac{1.201}{n} - 8\pi\left[K_o\left(\frac{2\pi c}{b}\right) + K_o\left(\frac{2\pi a}{b}\right)\right]\right\} \tag{B-7}$$

3. INTERACTION FIELDS FOR DIELECTRIC OBJECTS IN A TWO-DIMENSIONAL PERIODIC LATTICE

The two-dimensional periodic lattice considered here is illustrated in Figure B-4, where every dielectric object in the lattice has been replaced by its equivalent dipole moment p. To obtain the static interaction field of this lattice, we note that the three-dimensional interaction field of Equation (B-3) may be expressed in an alternative form as [6]

$$E_{yi} = \frac{p}{4\pi\varepsilon_2} \sum_{m=-\infty}^{\infty}{}' \sum_{n=-\infty}^{\infty} \sum_{s=-\infty}^{\infty} \frac{2(mb)^2 - (na)^2 - (sc)^2}{\left[(mb)^2 + (na)^2 + (sc)^2\right]^{5/2}} \tag{B-8}$$

In obtaining Equation (B-8), the following Poisson summation formula [6,17]

$$\sum_{n=-\infty}^{\infty} f(\gamma n) = \frac{1}{\gamma} \sum_{m=-\infty}^{\infty} F\left(\frac{2n\pi}{\gamma}\right) \tag{B-9}$$

has been appropriately applied where $F(\omega)$ is the Fourier transform of $f(t)$.

A comparison between Figure B-4 and Figure B-1 reveals that the interaction field for the two-dimensional lattice may be obtained from Equation (B-8) by omitting the summation over m. Again, using the Poisson summation formula and the approximation that the modified Bessel function $K_o(x)$ decreases rapidly as x increases, it can be shown that the interaction field

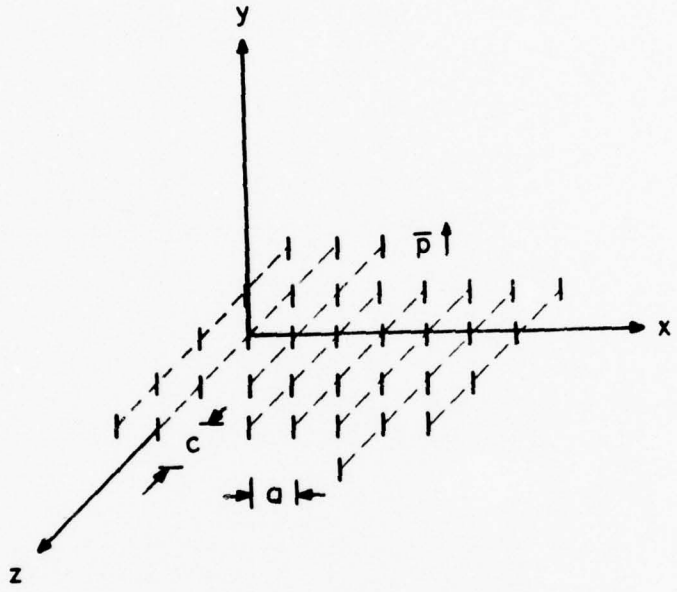

Fig. B-4 DIPOLE REPRESENTATION FOR DIELECTRIC OBJECTS IN A TWO-DIMENSIONAL LATTICE

at the center of the dielectric object for the two-dimensional lattice of Figure B-4 is given by

$$E_{yi} = \frac{\beta p}{\epsilon_2} \tag{B-10}$$

where β, the interaction constant, is

$$\beta \approx -\frac{1.201}{\pi}\left(\frac{1}{a^3}+\frac{1}{c^3}\right) + 8\pi\left[\left(\frac{1}{a^3}\right)K_o\left(\frac{2\pi c}{a}\right)+\left(\frac{1}{c^3}\right)K_o\left(\frac{2\pi a}{c}\right)\right] \tag{B-11}$$

APPENDIX C

DETERMINATION OF THE FIELDS INDUCED INSIDE THE BIOLOGICAL OBJECT FOR PARALLEL-PLATE SIMULATOR EXPERIMENTATION

1. INTRODUCTION

An analytical approach is described in this Appendix to the problem of determining the field induced inside the biological object (tissue) for the parallel-plate simulator experimentation at NMRI. The presentation is based on the analysis being generally applicable and not dependent on the specific details of the simulator system. The result can be used to calculate the electric field internal to the biological object for arbitrary dimensions of the simulator and for biological objects of any geometric shape, dimension and dielectric property. With the polarizability constant of the dielectric object (see Appendix A) and the static interaction constant in the periodic lattice (see Appendix B) obtained, this analytical development is accomplished by using the theory of artificial dielectric. Specifically, we wish to calculate the internal field within the biological objects in a periodic lattice in terms of the voltage applied between the two plates of the simulator as well as the physical characteristics and the electrical parameters of the biological object.

In this discussion, a realistic model for the simulator which neglects the distortion of the fringing field between the parallel plates has been adopted such that the field external to the periodic lattice is always uniform. This condition implies that the physical dimension of the parallel-plate simulator is larger than that of the periodic lattice.

2. EFFECTIVE PERMITTIVITY OF A PERIODIC LATTICE

2.1 Theoretical Basis

The geometrical construction for the parallel-plate simulator considered here is illustrated in Figure C-1. The biological objects under test are embedded in a homogeneous and isotropic dielectric slab in the form of a tissue culture tray. The permittivities of the biological objects (tissue) and its surrounding medium are designated by ε_1 and ε_2, respectively. The periodic lattice is exposed to a uniform electric field of very low frequency which, in the case of present interest, is generated by a parallel-plate. The periodic lattice with a height of ℓ_2 is located between the parallel plates at a distance ℓ_1 from the upper plate and ℓ_3 from the lower plate.

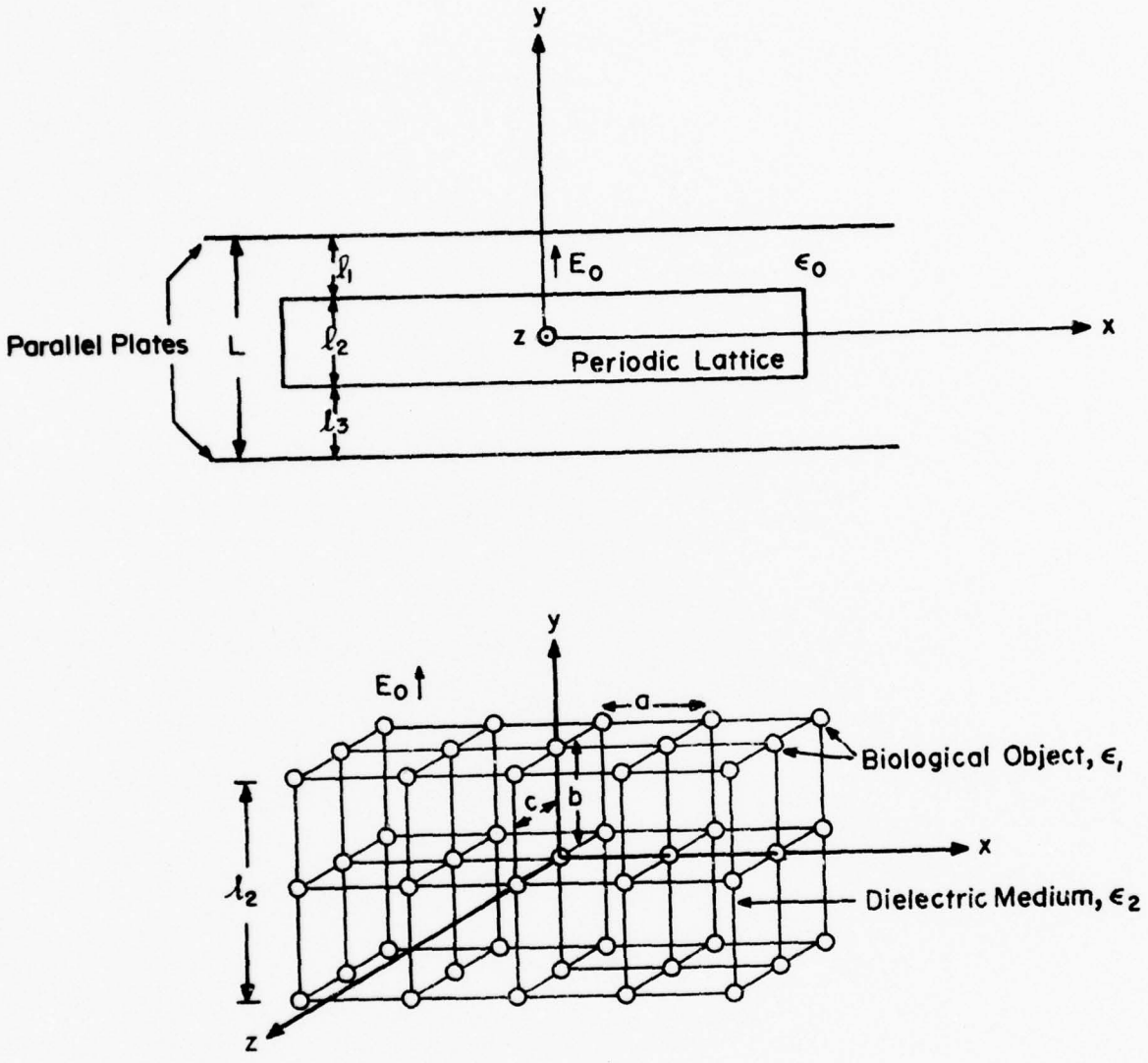

Fig. C.1 A PERIODIC LATTICE EXPOSED TO A UNIFORM ELECTRIC FIELD GENERATED BY A PARALLEL-PLATE SIMULATOR

Under the influence of E_o, electric charges are induced in the biological objects. Each object exhibits a dipole field. As a result, interaction occurs in the periodic lattice between all the dipole fields generated by the biological objects. The net combined effect, as has been used in the study of an artificial dielectric,[6,7] may be described, in terms of effective permittivity ε_e, by

$$D = \varepsilon_e E_p \tag{C-1}$$

where E_p denotes the electric field that would be induced in the periodic lattice.

Based on the theory of artificial dielectric, the effective permittivity for the periodic lattice of Figure C-1 may be expressed as[6]

$$\varepsilon_e = \varepsilon_2 \left\{ 1 + \frac{N\alpha_e}{1-\alpha_e\beta} \right\} \tag{C-2}$$

where α_e is the polarizability constant which characterizes the nature of the polarization under impressed electric fields in biological objects, N is the number of objects per unit volume and β is the interaction constant. In Appendix A, the polarizability constant has been discussed in detail for dielectric objects of various geometric shapes. The interaction constant β of a three-dimensional (or two-dimensional) periodic lattice has also been presented in Appendix B. The value of N in Equation (C-2) is equal to $(abc)^{-1}$ for the case of Figure C-1, where a, b, and c denote the spacings between the biological objects along the directions of x, y and z axes, respectively.

Provided ε_e is known, the electric field internal to the periodic lattice may then be obtained from

$$E_p = \frac{\varepsilon_o E_o}{\varepsilon_e} \tag{C-3}$$

where

$$E_o = \frac{V_o}{(\ell_1 + \ell_3) + \frac{\varepsilon_o}{\varepsilon_e}\ell_2} \tag{C-4}$$

and V_o is the applied voltage between the plates. In Equations (C-3) and (C-4) we have used the relation $V_o = (\ell_1+\ell_3)E_o+\ell_2E_p$ and the conservation of electric flux density (i.e., the normal component of D must be continuous at the surface boundary of the periodic lattice).

To illustrate the physical insight, it appears constructive to consider some special cases. For example, if the biological object considered here has the same permittivity as that of its surrounding medium $\varepsilon_1 = \varepsilon_2$, then the periodic lattice becomes a dielectric slab, as shown in Figure C-2(a). Under this condition, $\xi = \varepsilon_1/\varepsilon_2 = 1$ and $\alpha_e = 0$ (see Appendix A), we then have from Equation (C-2) that $\varepsilon_e = \varepsilon_2$ which, in turn, gives $E_{p,a} = \varepsilon_o E_o/\varepsilon_2$. This, as expected, is the solution of a dielectric slab with a permittivity ε_2 immersed in a uniform impressed electric field, E_o. Likewise, the electric field internal to the periodic lattice becomes $E_{p,b} = \varepsilon_o E_o/\varepsilon_1$ if the biological objects with a permittivity ε_1, shown in Figure C-2(b), are embedded in a dielectric having the same permittivity. Evidently, $E_{p,a}$ is larger than $E_{p,b}$, if $\varepsilon_1 > \varepsilon_2$. Therefore, we would expect that ε_e would have a value somewhat larger than ε_2 but smaller than ε_1, and that $E_{p,b} < E_p < E_{p,a}$.

2.2 Illustrative Example

As can be seen from Equation (C-2), the effective permittivity of a periodic lattice depends upon many parameters which include the permittivities of the biological object (ε_1) and its surrounding medium (ε_2), the size and shape of the object and the interaction constant. As an illustrative example, let us consider a three-dimensional periodic lattice of Figure C-1. The lattice consists of a large number of biological objects which are embedded in a dielectric (or plastic) slab. The geometry of the object is taken to be a prolate spheroid. In this example, we use

a = 3/8 inch, the lattice element spacing along the direction of x-axis;

b = 19/32 inch, the lattice element spacing along the direction of y-axis;

c = 3/8 inch, the lattice element spacing along the direction of z-axis;

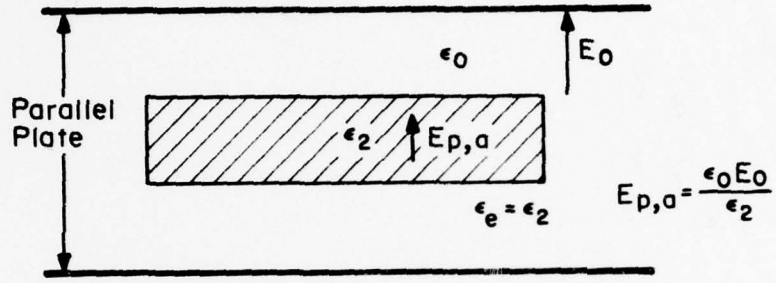

(a)

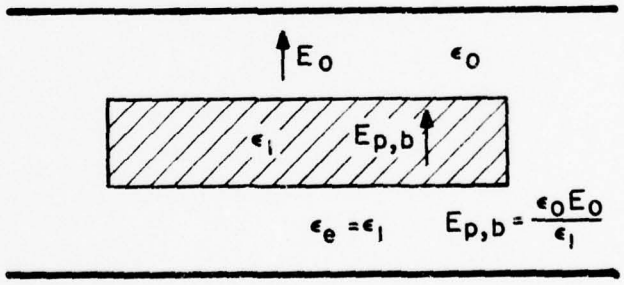

(b)

Fig. C-2, DIELECTRIC SLAB IN A UNIFORM ELECTRIC FIELD.

r_a = 1/4 inch, the major radius of the prolate biological object;

r_b = 1/8 inch, the minor radius of the prolate biological object.

When exposed to a uniform ELF electric field, the interaction constant, from Equation (B-7) in Appendix B, is obtained to be $\beta \approx -0.62/\pi b^3$. The insertion of β in Equation (C-2) results in the effective permittivity for the periodic lattice

$$\varepsilon_e \cong \varepsilon_2 \left\{ \frac{1 + 0.211\ (\xi-1)/\Delta}{1 + 0.015\ (\xi-1)/\Delta} \right\} \tag{C-5}$$

where

$$\Delta = \left\{ 1+(\xi-1)(u^2-1)\left[u \coth^{-1}(u) - 1 \right] \right\}$$

$$u = \frac{1}{\left[1-(r_b/r_a)^2 \right]^{1/2}} \tag{C-6}$$

Figure C-3 shows the normalized effective permittivity (with respect to ε_2) obtained from Equations (C-5) and (C-6). The normalized effective permittivity is plotted as a function of the ratio $\xi = \varepsilon_1/\varepsilon_2$.

If $\varepsilon_1 > \varepsilon_2$, the effective permittivity of the periodic lattice, as mentioned previously, always has a value larger than ε_2 but smaller than ε_1. This is evidenced from Figure C-3. The effective permittivity for the periodic lattice at $\xi = 20$, for example, has a value which is about 1.99 times larger than ε_2, but is approximately 10 times smaller than ε_1. When $\varepsilon_1 = \varepsilon_2$, no biological object exists in the lattice. In this case, Equation (C-4) as well as Figure C-3, as expected, predict that $\varepsilon_e = \varepsilon_1 = \varepsilon_2$.

3. INDUCED ELECTRIC FIELD INTERNAL TO THE BIOLOGICAL OBJECTS IN A PERIODIC LATTICE

3.1 General Formulation of the Problem

When the periodic lattice is exposed to a uniform electric field E_o, electric charges are induced in the biological objects. The charges in the objects are displaced to set up an induced field that will eventually satisfy the boundary conditions at the object surface. Each object thus exhibits a dipole field and, hence, interaction occurs. At extremely low frequencies

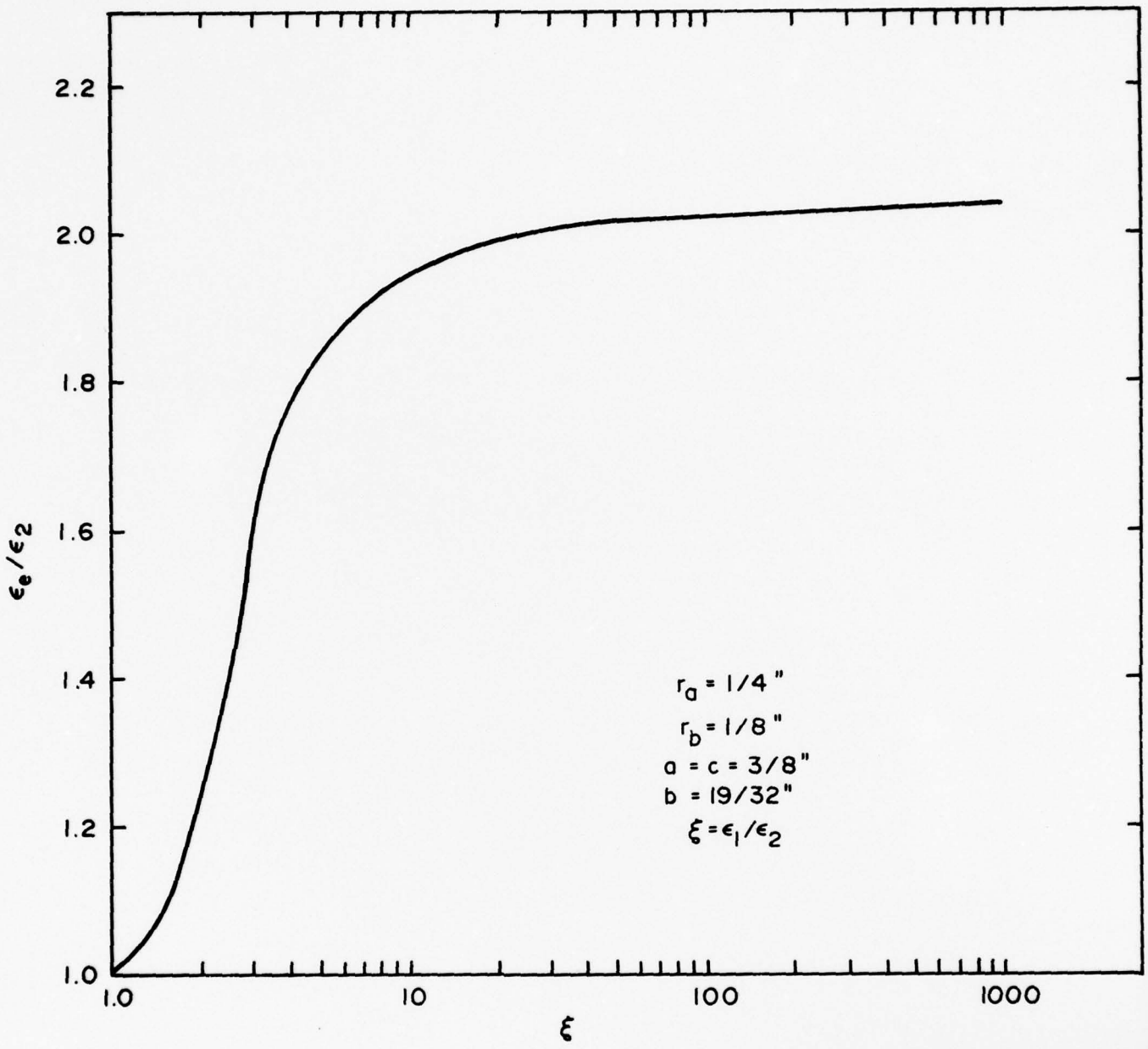

Fig. C-3 VARIATION IN EFFECTIVE PERMITTIVITY FOR A THREE-DIMENSIONAL PERIODIC LATTICE

where the wavelength is long compared to the dimension of the object, the electric field acting to polarize any object, therefore, may be assumed to be a uniform field equal to the field at the center of the object. The field, from the considerations of the symmetric geometry of Figure C-1, has only a y-directed component. The total combined effect of all the biological objects in the periodic lattice is to produce a new average dipole polarization, P, for the medium. This basic mechanism may be best described by the Lorentz theory in which the electric flux density, D, (given by Equation (C-1)) consists of two parts; the first part relates the electric field to the medium permittivity, ε_2, and the second part is called the dipole polarization. That is

$$D = \varepsilon_2 E_p + P \tag{C-7}$$

From this expression as well as Equations (C-1) and (C-2), it becomes straightforward to obtain the new average dipole moment, p, (i.e., P/N where N = abc)

$$p = \frac{\alpha_e \varepsilon_2}{1-\alpha_e \beta} E_p. \tag{C-8}$$

Inserting E_p, given by Equation (C-3), into Equation (C-8), the dipole moment, p, may also be expressed in terms of V_o, the applied voltage between the upper and lower plates of the simulator, as

$$p = \left\{\frac{\alpha_e \varepsilon_2}{1-\alpha_e \beta}\right\} \left\{\frac{V_o}{\left[\ell_2+(\ell_1+\ell_3)(\varepsilon_e/\varepsilon_o)\right]}\right\} \tag{C-9}$$

To determine the electric field strength induced internal to the biological objects in a periodic lattice, we note that the dipole moment, p, as defined by Stratton,[8] is related by the internal electric field, E_i, by

$$p = k_v(\varepsilon_1-\varepsilon_2) E_i \tag{C-10}$$

where k_v is the volume of the object, since the polarization is defined as the dipole moment, p, per unit volume. Using the expression of Equation (C-9) which is the total dipole moment including the effect of (dipole) field interactions, we have

$$E_i = \left\{\frac{\alpha_e}{(1-\alpha_e\beta)k_v}\right\}\left\{\frac{V_o/(\xi-1)}{\left[\ell_2+(\ell_1+\ell_3)(\varepsilon_e/\varepsilon_o)\right]}\right\} \qquad \text{(C-11)}$$

for the electric field induced inside the biological object when the periodic lattice is exposed to a uniform electric field generated by a parallel plate voltage, V_o.

From the polarizability constants listed in Table A-2 in Appendix A, the expression of Equation (C-11) reveals that if $\varepsilon_1 = \varepsilon_2$ (i.e. $\xi = 1$, $\varepsilon_e = \varepsilon_1 = \varepsilon_2$), the induced electric field internal to the biological object for any geometric shape becomes $E_i = V_o/\left[\ell_2+(\ell_1+\ell_3)\varepsilon_1/\varepsilon_o\right]$, which, as expected, is the result obtained from a dielectric slab situated between the parallel plate.

3.2 Parametric Results

In this section, sample calculations for the induced electric field internal to the biological objects in a periodic lattice are presented. The calculation is based on Equation (C-11). Note that the value of ε_1, the permittivity of the biological object, employed here is for exploratory parametric calculations, and is different from that used in the text where the permittivity for a high water content biological tissue is used.

We first consider the three-dimensional lattice. Calculations have been carried out for dielectric objects of three geometric shapes; prolate spheroid, sphere and finite circular cylinder. In each case, the dimension of the dielectric object is properly chosen such as to have the same volume. Note that the resultant expression for the polarization constant obtained in Appendix A for a long thin cylinder is used for the finite cylindrical dielectric object. The results for the finite cylinder model of dielectric objects, therefore, are approximate, but are included here for comparison. In this calculation, the following notations and parameters are used:

a = 3/8 inch, the lattice element spacing along the direction of x-axis;

b = 19/32 inch, the lattice element spacing along the direction of y-axis;

c = 3/8 inch, the lattice element spacing along the direction of z-axis;

r_a = 1/4 inch, the major radius of the prolate spheroidal dielectric object;

r_b = 1/8 inch, the minor radius of the prolate spheroidal dielectric object;

r_o = 5/32 inch, the radius of the dielectric sphere.

r_e = 1/8 inch, the radius of the finite cylindrical dielectric object;

h = 7/16 inch, the height of the finite cylindrical dielectric object;

ℓ_1 = spacing between the periodic lattice and the upper plate of the simulator;

ℓ_2 = height of the periodic lattice;

ℓ_3 = spacing between the periodic lattice and the lower plate of the simulator;

L = separation between the upper and lower plates of the simulator;

ε_1 = 81 ε_o, the permittivity of the dielectric object, where $\varepsilon_o = 10^{-9}/36\pi$ farads/m;

ε_2 = 2.25 ε_o farads/m, the permittivity of the dielectric slab in which dielectric objects are embedded;

ξ = $\varepsilon_1/\varepsilon_2$;

V_o = voltage applied between the plates of the simulator.

The calculated results, obtained for the case of $\ell_1 = \ell_3 = L/4$, $\ell_2 = L/2$, are graphically presented in Figures C-4 to C-6 for the sphere, prolate spheroid and finite cylinder dielectric objects, respectively. In the figure, the induced internal electric field is normalized to (V_o/L).

We now consider the two-dimensional periodic lattice. The dielectric objects are embedded in a dielectric slab in the x-z plane (see Figure C-1) with lattice spacings a and c along the x and z directions, respectively. In this case, the height of the lattice is taken to be ℓ_2 = 19/32".

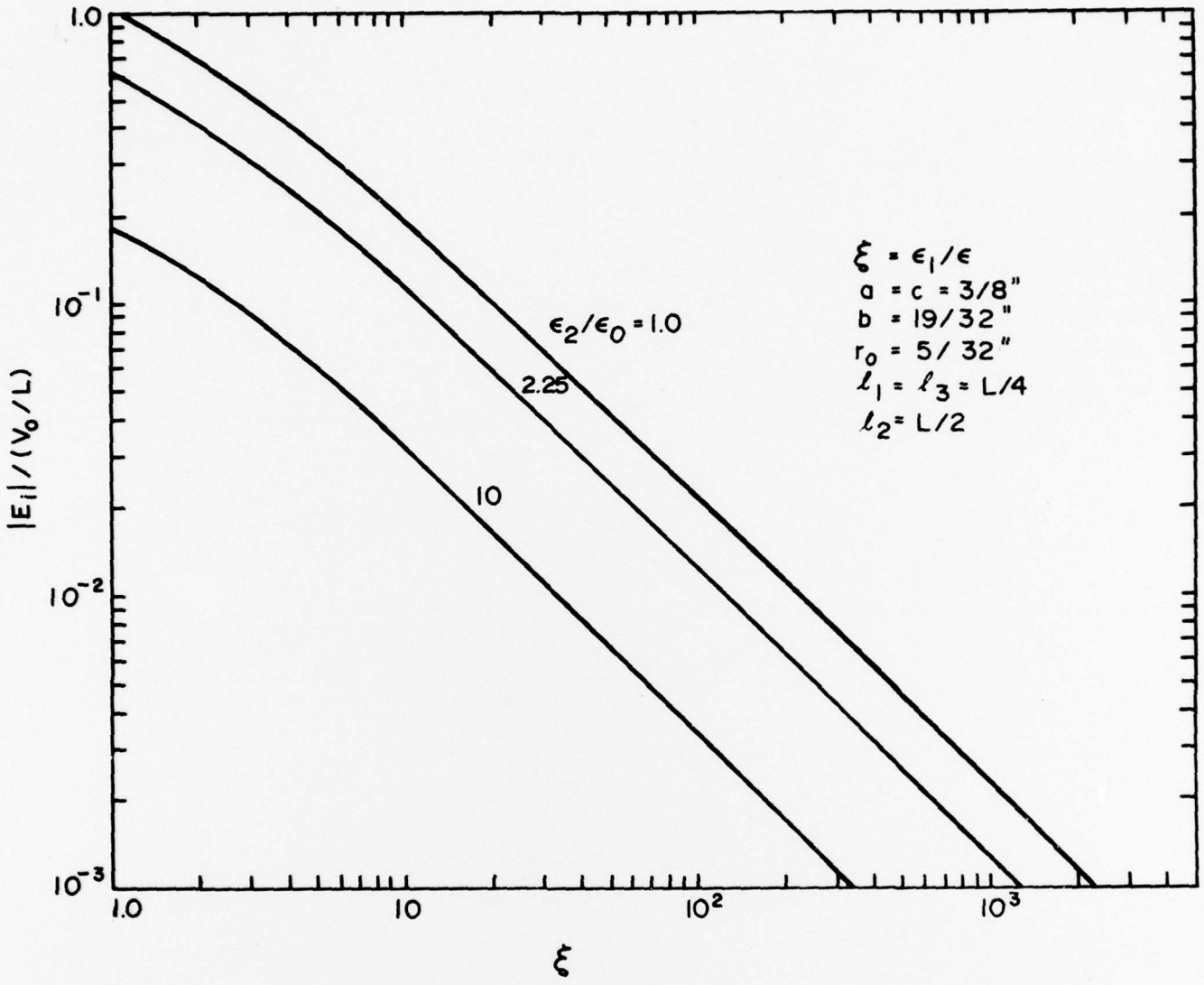

Fig. C-4 INDUCED ELECTRIC FIELD INTERNAL TO DIELECTRIC SPHERES IN A THREE-DIMENSIONAL PERIODIC LATTICE

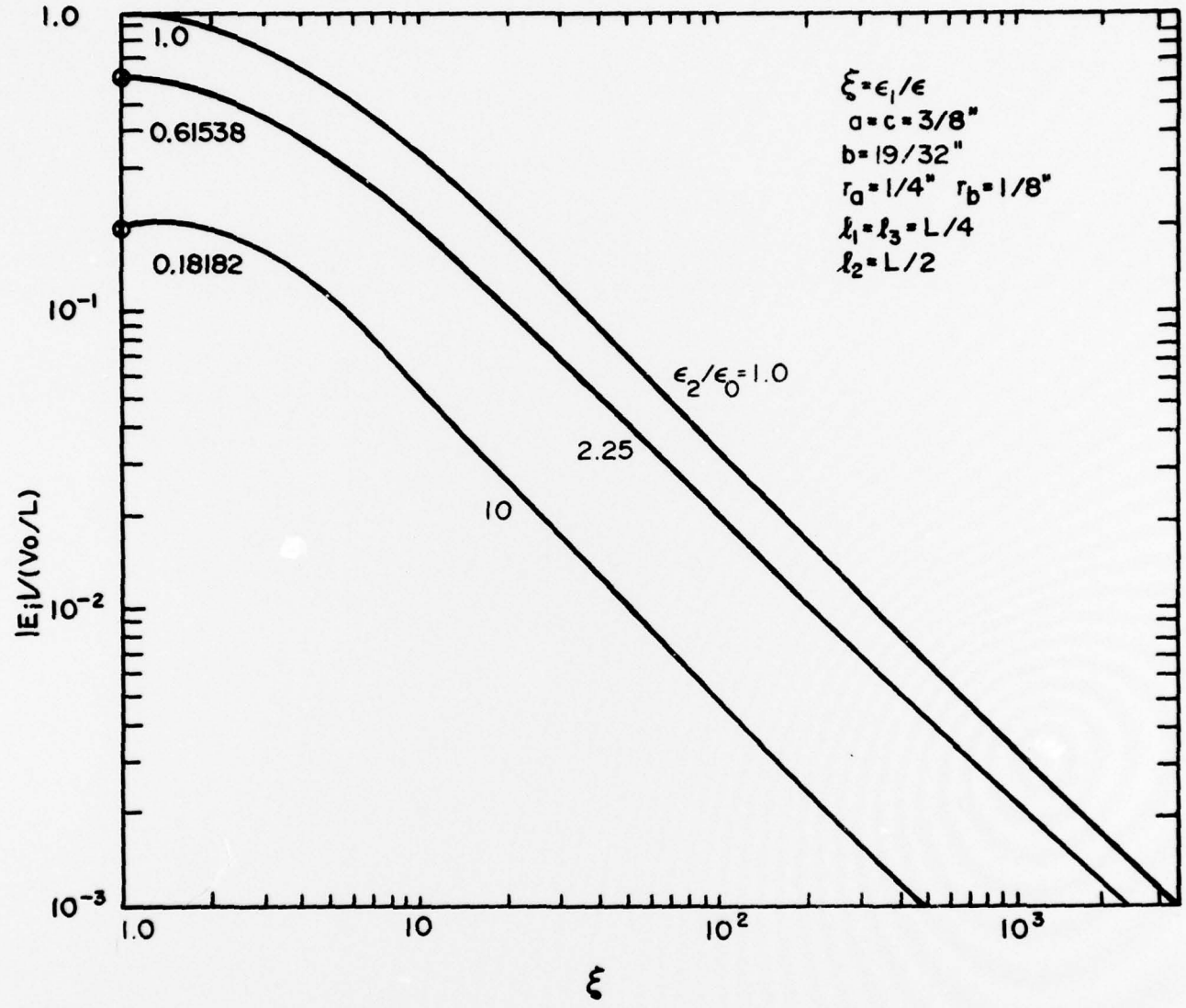

Fig. C-5 INDUCED ELECTRIC FIELD INTERNAL TO PROLATE DIELECTRIC SPHEROIDS IN A THREE-DIMENSIONAL PERIODIC LATTICE

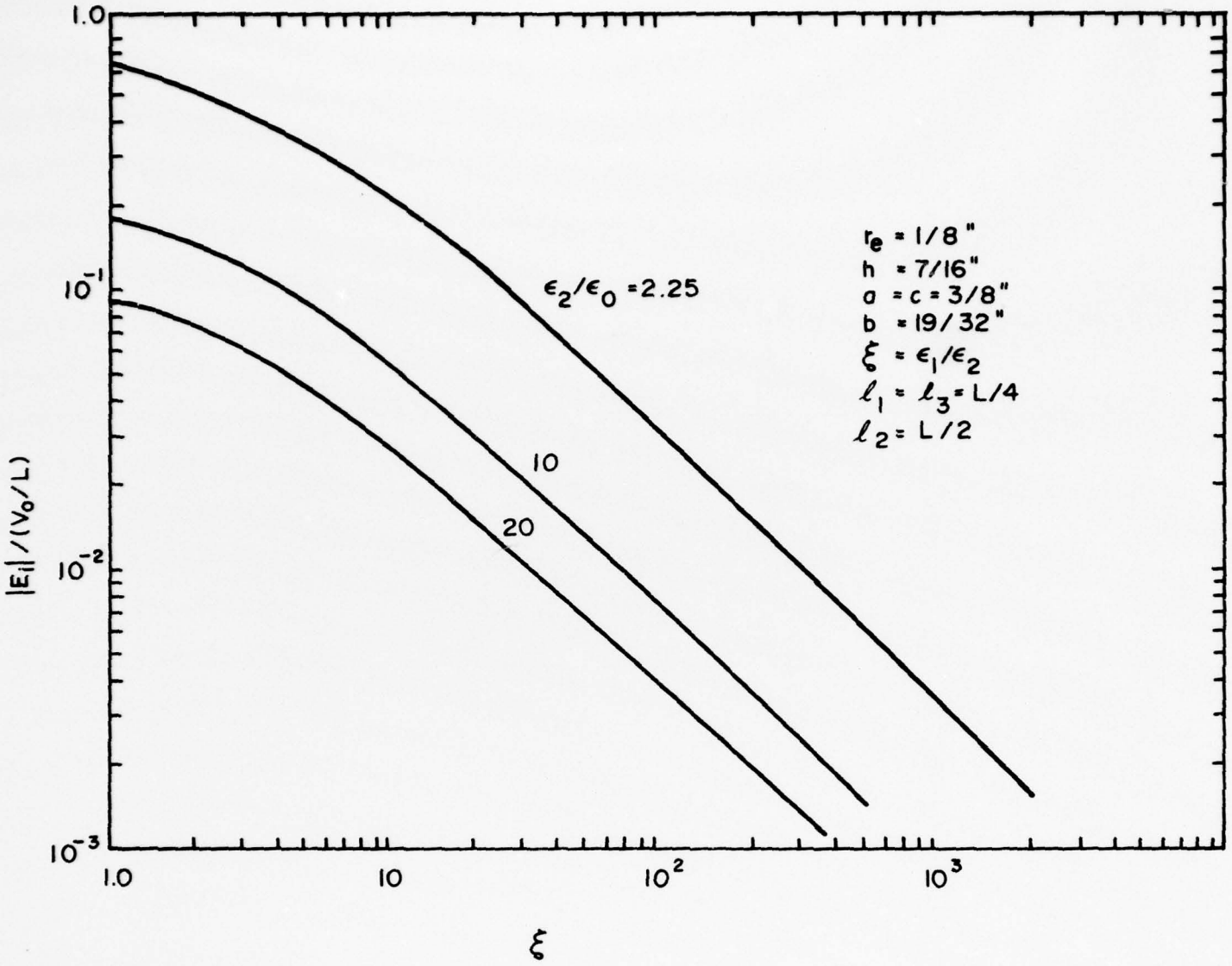

Fig. C-6 INDUCED ELECTRIC FIELD INTERNAL TO FINITE CYLINDRICAL DIELECTRIC OBJECTS IN A THREE-DIMENSIONAL PERIODIC LATTICE

Based on the two-dimensional interaction constant, given by Equation (B-11) in Appendix B, the induced internal electric fields are calculated for dielectric objects of prolate spheroid, sphere and finite cylinder. The results are presented in Figures C-7 to C-9 for the case when $\ell_1 = \ell_3 = 2L/5$ and $\ell_2 = L/5$.

One lattice structure of relative importance is the cubic array consisting of identical spheres with a radius r_o. As a cubic array, the lattice element spacings are simply a = b = c. Shown in Figure C-10 is the induced internal electric field for the case when $\ell_1 = \ell_3 = L/4$ and $\ell_2 = L/2$. The induced electric field is plotted as a function of the relative permittivity $\varepsilon_2/\varepsilon_o$ for two values of ξ ($= \varepsilon_1/\varepsilon_2$).

4. REMARKS

Simple expressions have been obtained for the induced electric field internal to the biological objects of either a three-dimensional or a two-dimensional periodic lattice. The discussion is based on the theory of artificial dielectric. A limitation of this simple theory is that the object size and the element spacing must be small, being not greater than 0.1 of a wavelength. For our present problem at extremely low frequencies, the results should provide sufficient accuracy, because the dimension of the biological objects and their element spacing are, indeed, very small compared to a wavelength.

The presentation given in this Appendix is based on the analysis being generally applicable to many problem areas, and not dependent upon the specific details of the simulator, lattice structures, and the geometric shape of the objects. Hence, the results are useful in the study of electromagnetic coupling and interference, electromagnetic biological effects and biomedical testings, slotted waveguide arrays and artificial dielectrics.

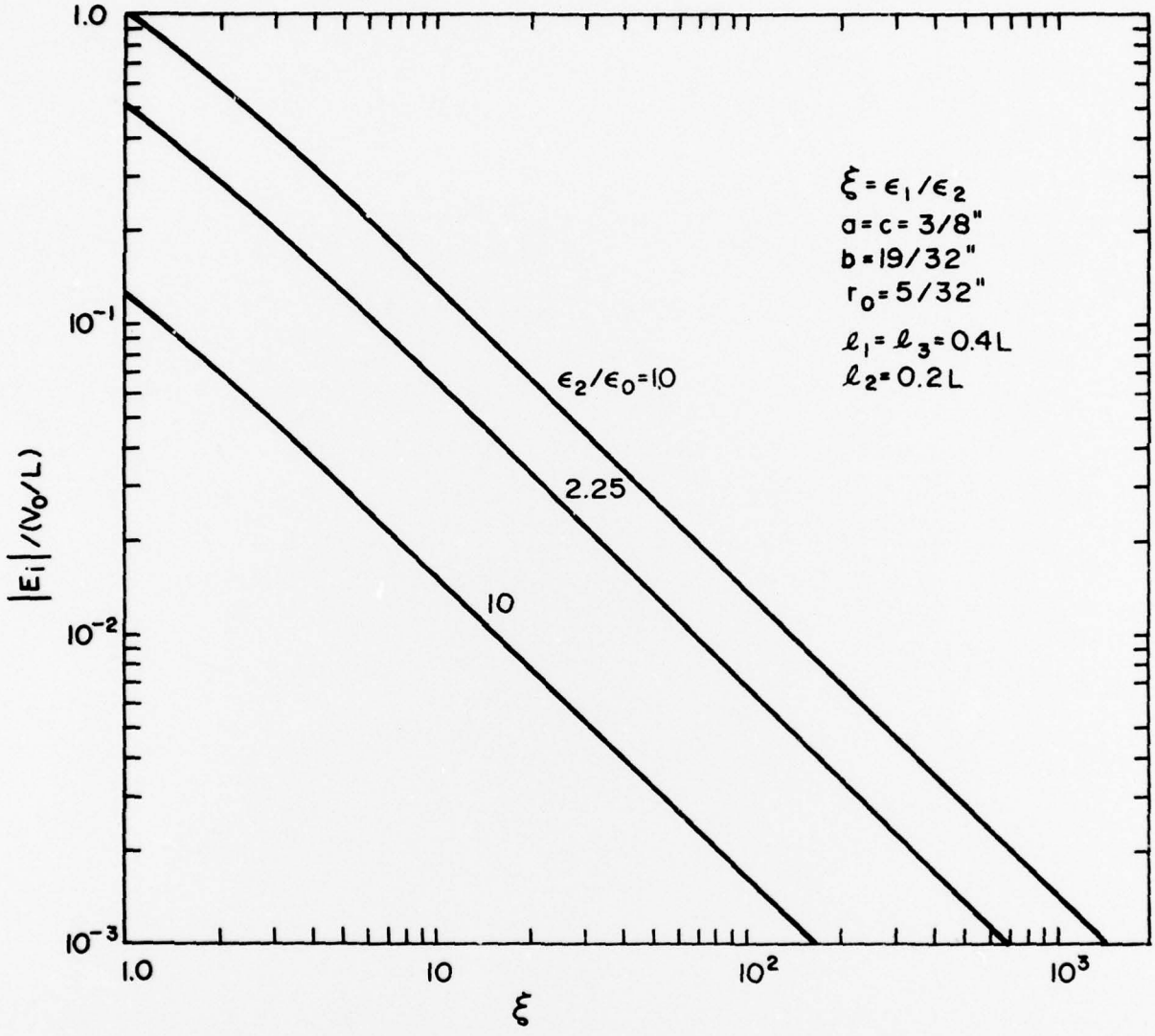

Fig. C-7 INDUCED ELECTRIC FIELD INTERNAL TO DIELECTRIC SPHERES IN A TWO-DIMENSIONAL PERIODIC LATTICE

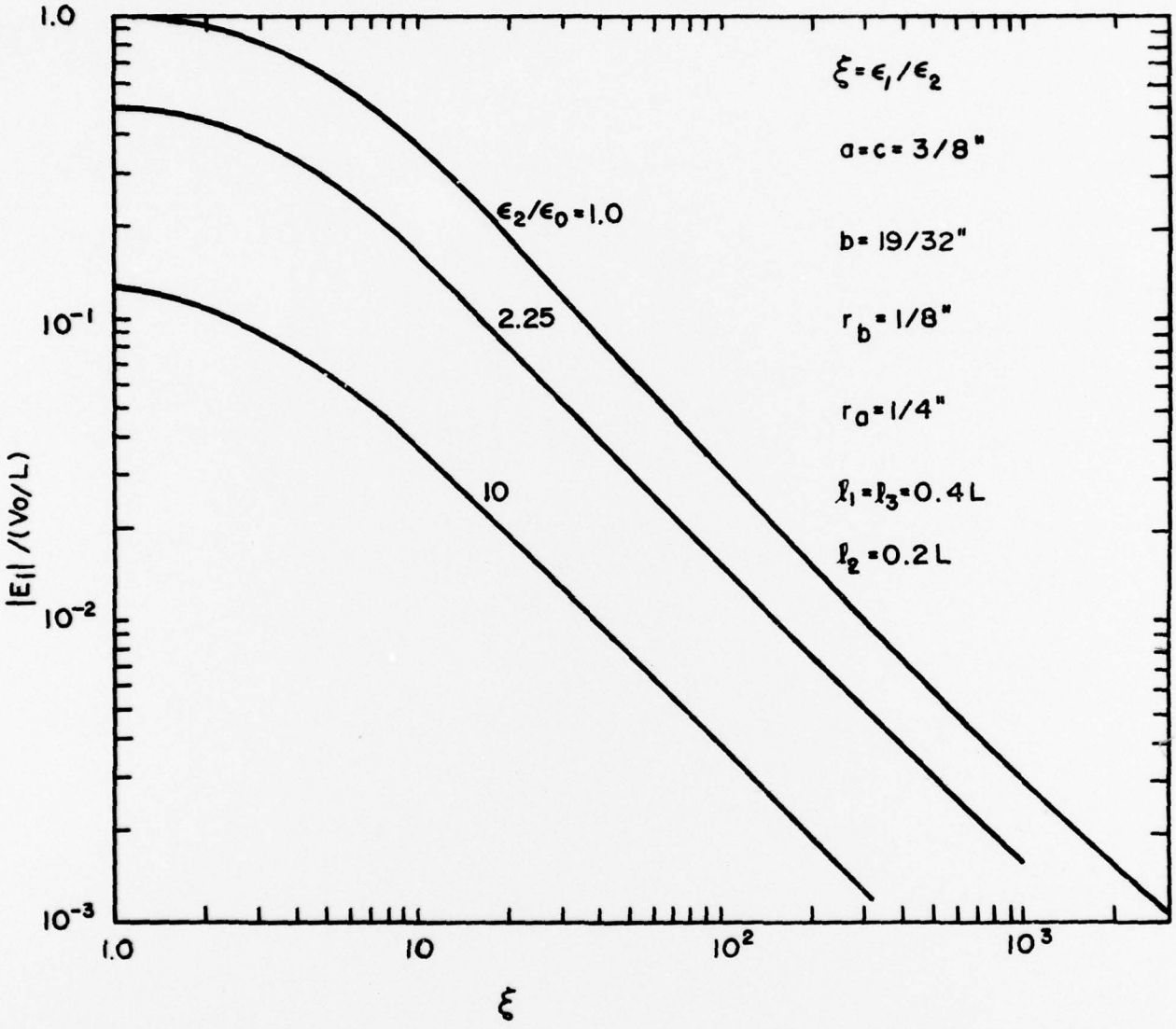

Fig. C-8 INDUCED ELECTRIC FIELD INTERNAL TO PROLATE DIELECTRIC SPHEROIDS IN A TWO-DIMENSIONAL PERIODIC LATTICE

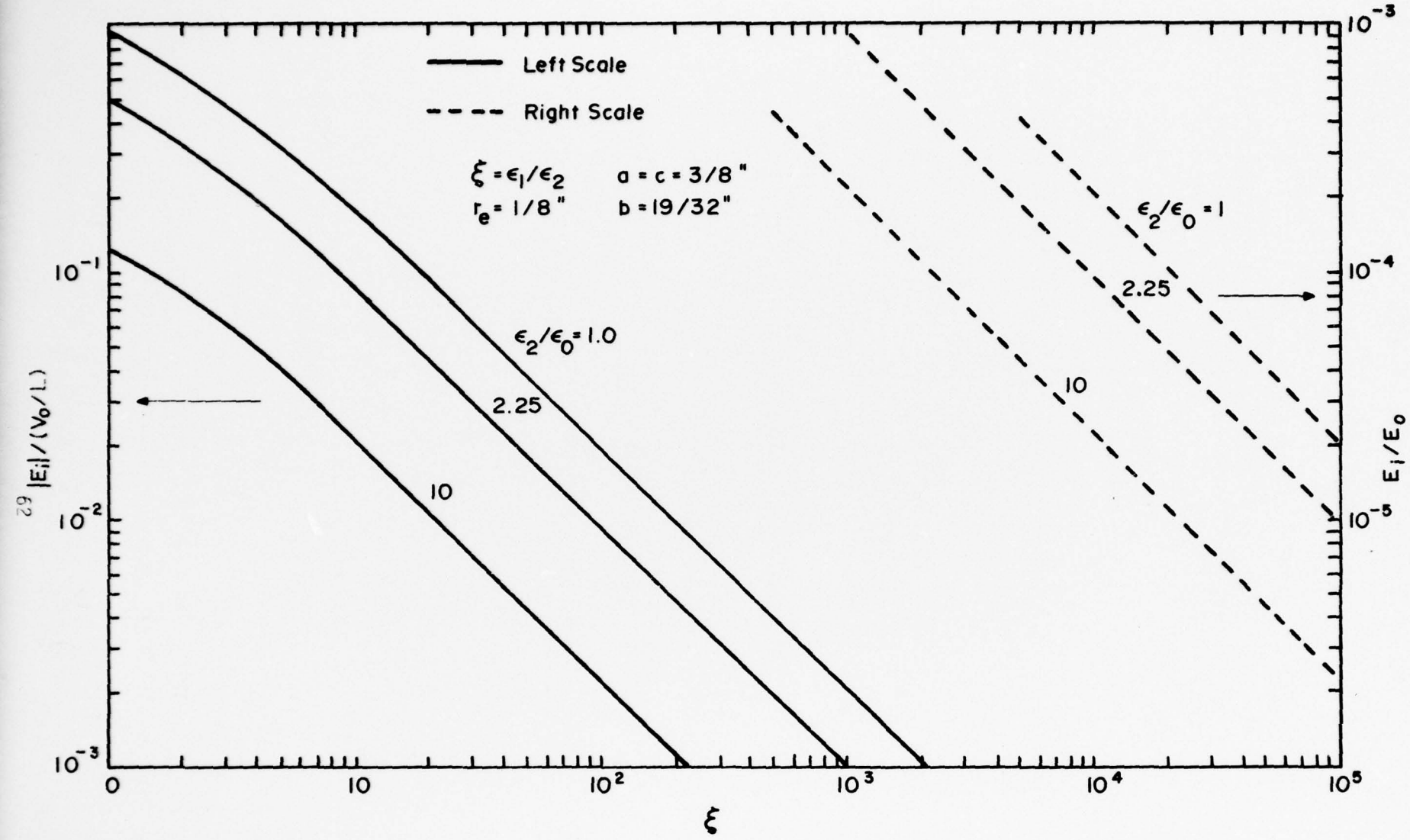

Fig. C-9 INDUCED ELECTRIC FIELD INTERNAL TO FINITE CYLINDRICAL DIELECTRIC OBJECTS IN A TWO-DIMENSIONAL LATTICE

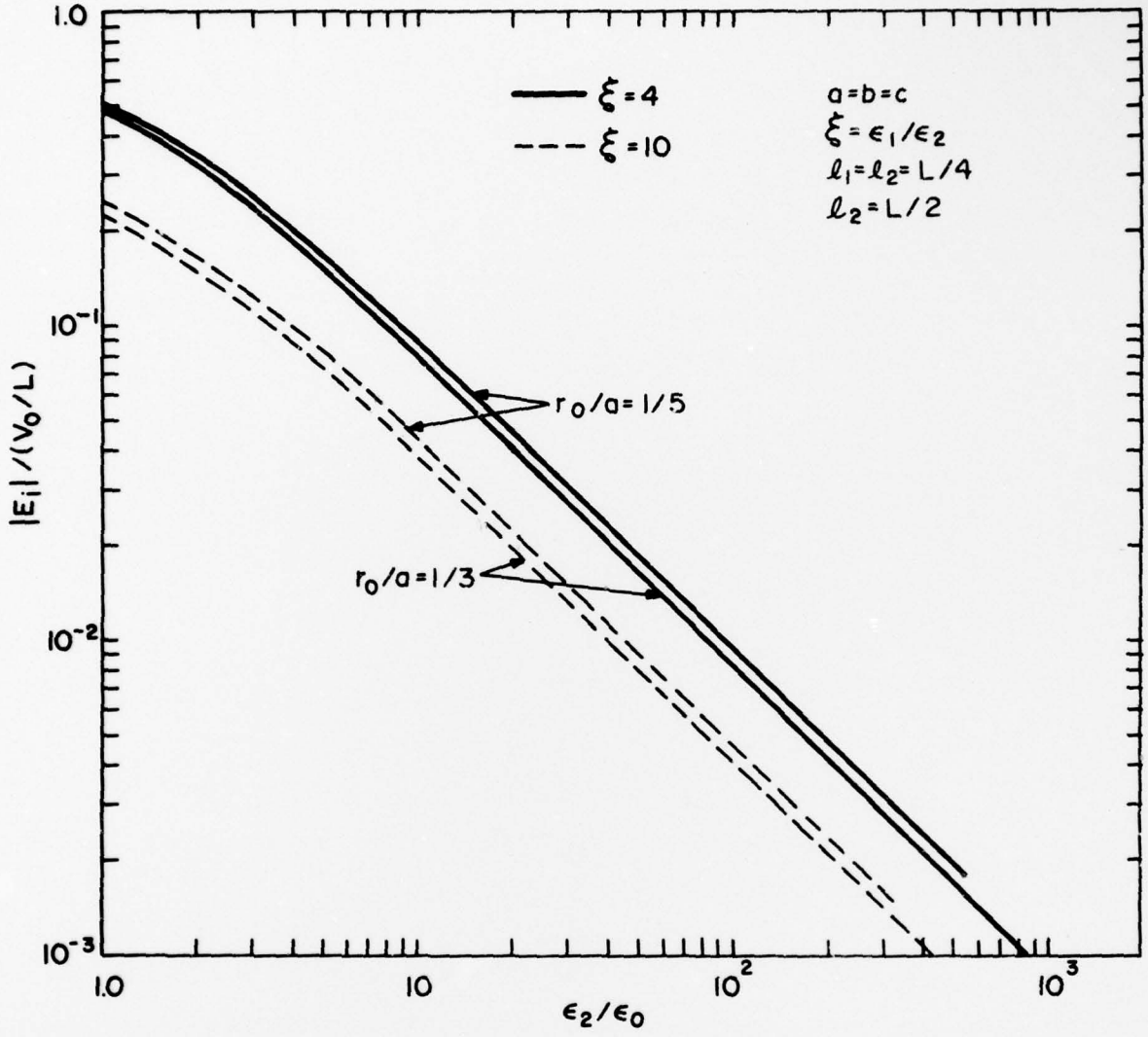

Fig. C-10 INDUCED ELECTRIC FIELD INTERNAL TO DIELECTRIC SPHERES IN A CUBIC PERIODIC LATTICE.

REFERENCES

1. S. M. Michaelson, "Human Exposure to Nonionizing Radiant Energy - Potential Hazards and Safety Standards," Proc. IEEE, Vol. 60, pp. 389-421, April 1972.

2. M. H. Benedick and B. Greenberg, "The Sanguine Biological-Ecological Research Program," IEEE Transactions on Communications, Vol. COM-22, No. 4, April 1974.

3. Seafarer ELF Communications System Draft Environmental Impact Statement for Site Selection and Test Operations, Appendix E: Biological Ecological Information, February 1977.

4. Electric Power Research Institute, Biological Effects of High Voltage Electric Fields, EPRI 381-1, Final Report, November 1975.

5. J. Gauger, ELF Electric and Magnetic Field Simulation for a Laboratory Biological Experiment, Technical Report No. 10, Project E6357, IIT Research Institute, July 1977.

6. R. E. Collin, Field Theory and Guided Waves (New York, N.Y.: McGraw-Hill Book Company, 1960), Chapter 12.

7. J. Brown and W. Johnson, "The Relative Permittivity of Tetragonal Arrays of Perfectly Conducting Thin Disks," Proc. IEE., Vol. 102, Pt. B, pp. 37-42, January 1955.

8. J. A. Stratton, Electromagnetic Theory (New York, N.Y.: McGraw-Hill Book Company, 1941).

9. R. E. Collins and W. H. Eggimann, "Dynamic Interaction Fields in a Two-Dimensional Lattice," IRE Trans. on Microwave Theory and Techniques, Vol. MTT-9, pp. 110-115, March 1961.

10. H. P. Schwan, "Electrical Properties of Tissue and Cells," Adv. Biol. Med. Phys., Vol. 5, pp. 147-209, 1975.

11. C. C. Johnson and A. W. Guy, "Nonionized Electromagnetic Wave Effects in Biological Materials and Systems," Proc. IEEE, Vol. 60, pp. 692-718, June 1972.

12. R. J. Spiegel, "ELF Coupling to Spherical Models of Man and Animals," IEEE Trans. on Biomedical Engineering, Vol. BME-23, No. 5, pp. 387-391, September 1976.

13. J. C. Lin, A. W. Guy, and C. C. Johnson, "Power Deposition in a Spherical Model of Man Exposed to 1-20 MHz Electromagnetic Fields," IEEE Trans. on Microwave Theory and Techniques, Vol. MTT-21, No. 12, pp. 791-797, December 1973.

14. W. R. Smyth, Static and Dynamic Electricity (New York, N.Y.: McGraw-Hill Book Company, 1950) pp. 67-68.

15. Y. Shiau and A. R. Valentino, ELF Electric Field Coupling to Dielectric Spheroids, Technical Report, IITRI Project No. E6320, BRH Contract No. 223-75-6012, July 1976.

16. H. B. Dwight, Table of Integrals and Other Mathematical Data (New York, N.Y.: The MacMillan Company, 1967) p. 12.

17. D. K. Cheng, Analysis of Linear Systems (Reading, Massachusetts: Addison-Wesley Publishing Company, Inc., 1961) pp. 304-305.

Unclassified

SECURITY CLASSIFICATION OF THIS PAGE (When Data Entered)

REPORT DOCUMENTATION PAGE		READ INSTRUCTIONS BEFORE COMPLETING FORM
1. REPORT NUMBER	2. GOVT ACCESSION NO.	3. RECIPIENT'S CATALOG NUMBER
4. TITLE (and Subtitle) ELF Electric Field Analysis for a Laboratory Biological Experiment		5. TYPE OF REPORT & PERIOD COVERED Technical 6. PERFORMING ORG. REPORT NUMBER TR E6357-9
7. AUTHOR(s) Y. Shiau		8. CONTRACT OR GRANT NUMBER(s) N00039-76-C-0141
9. PERFORMING ORGANIZATION NAME AND ADDRESS IIT Research Institute 10 W. 35th Street Chicago, IL 60616		10. PROGRAM ELEMENT, PROJECT, TASK AREA & WORK UNIT NUMBERS
11. CONTROLLING OFFICE NAME AND ADDRESS Naval Electronic Systems Command Washington, DC 20360		12. REPORT DATE May 1978 13. NUMBER OF PAGES 65
14. MONITORING AGENCY NAME & ADDRESS(If different from Controlling Office)		15. SECURITY CLASS. (of this report) Unclassified 15a. DECLASSIFICATION/DOWNGRADING SCHEDULE

16. DISTRIBUTION STATEMENT (of this Report)

Unlimited Distribution

17. DISTRIBUTION STATEMENT (of the abstract entered in Block 20, If different from Report)

18. SUPPLEMENTARY NOTES

19. KEY WORDS (Continue on reverse side if necessary and identify by block number)

Extremely Low Frequency
Electromagnetic Field
Electromagnetic Radiation
Electromagnetic Coupling
Biological Effects
Tissue Cultures
Induced Electric Field
Electric Field Analysis
Electric Field Simulation
Sanguine
Seafarer
ELF Communications

20. ABSTRACT (Continue on reverse side if necessary and identify by block number)

This technical report is intended to support biological studies in connection with the Navy's Proposed ELF communications system. The report covers an analysis of the electric field levels induced in individual tissue culture samples when exposed to uniform electric and magnetic fields in a laboratory simulator. Calculations are included to derive sample electric field levels for a tissue culture experiment.

DD FORM 1 JAN 73 1473 EDITION OF 1 NOV 65 IS OBSOLETE

Unclassified